NASA/CR–2014-218521

AFC-Enabled Simplified High-Lift System Integration Study

Peter M. Hartwich, Eric D. Dickey, Anthony J. Sclafani, Peter Camacho,
Antonio B. Gonzales, Edward L. Lawson, Ron Y. Mairs, and Arvin Shmilovich
The Boeing Company, Huntington Beach, California

September 2014

NASA STI Program . . . in Profile

Since its founding, NASA has been dedicated to the advancement of aeronautics and space science. The NASA scientific and technical information (STI) program plays a key part in helping NASA maintain this important role.

The NASA STI program operates under the auspices of the Agency Chief Information Officer. It collects, organizes, provides for archiving, and disseminates NASA's STI. The NASA STI program provides access to the NASA Aeronautics and Space Database and its public interface, the NASA Technical Report Server, thus providing one of the largest collections of aeronautical and space science STI in the world. Results are published in both non-NASA channels and by NASA in the NASA STI Report Series, which includes the following report types:

- TECHNICAL PUBLICATION. Reports of completed research or a major significant phase of research that present the results of NASA Programs and include extensive data or theoretical analysis. Includes compilations of significant scientific and technical data and information deemed to be of continuing reference value. NASA counterpart of peer-reviewed formal professional papers, but having less stringent limitations on manuscript length and extent of graphic presentations.

- TECHNICAL MEMORANDUM. Scientific and technical findings that are preliminary or of specialized interest, e.g., quick release reports, working papers, and bibliographies that contain minimal annotation. Does not contain extensive analysis.

- CONTRACTOR REPORT. Scientific and technical findings by NASA-sponsored contractors and grantees.

- CONFERENCE PUBLICATION. Collected papers from scientific and technical conferences, symposia, seminars, or other meetings sponsored or co-sponsored by NASA.

- SPECIAL PUBLICATION. Scientific, technical, or historical information from NASA programs, projects, and missions, often concerned with subjects having substantial public interest.

- TECHNICAL TRANSLATION. English-language translations of foreign scientific and technical material pertinent to NASA's mission.

Specialized services also include organizing and publishing research results, distributing specialized research announcements and feeds, providing information desk and personal search support, and enabling data exchange services.

For more information about the NASA STI program, see the following:

- Access the NASA STI program home page at *http://www.sti.nasa.gov*

- E-mail your question to help@sti.nasa.gov

- Fax your question to the NASA STI Information Desk at 443-757-5803

- Phone the NASA STI Information Desk at 443-757-5802

- Write to:
  STI Information Desk
  NASA Center for AeroSpace Information
  7115 Standard Drive
  Hanover, MD 21076-1320

NASA/CR–2014-218521

AFC-Enabled Simplified High-Lift System Integration Study

Peter M. Hartwich, Eric D. Dickey, Anthony J. Sclafani, Peter Camacho,
Antonio B. Gonzales, Edward L. Lawson, Ron Y. Mairs, and Arvin Shmilovich
The Boeing Company, Huntington Beach, California

National Aeronautics and
Space Administration

Langley Research Center
Hampton, Virginia 23681-2199

Prepared for Langley Research Center
under Contract NNL10AA05B

September 2014

Acknowledgments

This study was carried out under NASA Contract: NNL10AA05B / NNL13AB65T. Dr. John Lin was the NASA LaRC Task Principal Investigator. In addition to the authors, the following Boeing personnel contributed to this work: J. Courtney, D. Lacy, Y. Yadlin, J.C. Vassberg, and E. Whalen.

Available from:

NASA Center for AeroSpace Information
7115 Standard Drive
Hanover, MD 21076-1320
443-757-5802

Abstract

The primary objective of this trade study report is to explore the potential of using Active Flow Control (AFC) for achieving lighter and mechanically simpler high-lift systems for transonic commercial transport aircraft. This assessment was conducted in four steps. First, based on the Common Research Model (CRM) outer mold line (OML) definition, two high-lift concepts were developed. One concept, representative of current production-type commercial transonic transports, features leading edge slats and slotted trailing edge flaps with Fowler motion. The other CRM-based design relies on drooped leading edges and simply hinged trailing edge flaps for high-lift generation.

The relative high-lift performance of these two high-lift CRM variants is established using Computational Fluid Dynamics (CFD) solutions to the Reynolds-Averaged Navier-Stokes (RANS) equations for steady flow. These CFD assessments identify the high-lift performance that needs to be recovered through AFC to have the CRM variant with the lighter and mechanically simpler high-lift system match the performance of the conventional high-lift system.

Conceptual design integration studies for the AFC-enhanced high-lift systems were conducted with a NASA Environmentally Responsible Aircraft (ERA) reference configuration, the so-called ERA-0003 concept. These design trades identify AFC performance targets that need to be met to produce economically feasible ERA-0003-like concepts with lighter and mechanically simpler high-lift designs that match the performance of conventional high-lift systems.

Finally, technical challenges are identified associated with the application of AFC-enabled high-lift systems to modern transonic commercial transports for future technology maturation efforts.

Nomenclature

α	Angle of attack
AFC	Active Flow Control
AFRL	Air Force Research Laboratory
AIAA	American Institute of Aeronautics & Astronautics
APU	Auxiliary Power Unit
ATT	Advanced Tactical Theater
CFD	Computational Fluid Dynamics
CRM	Common Research Model
DLR	Deutsche Luft & Raumfahrt (German Air & Space)
ERA	Environmentally Responsible Aircraft
LE	Leading edge
MADCAP	Modular Aerodynamic Computational Analysis Process
NFAC	National Full Scale Aerodynamic Complex
lNPV	Net Present Value

OEW	Overall Empty Weight
QFD	Quality Function Deployment
RANS	Reynolds-Averaged Navier–Stokes
TE	Trailing edge
TOD	Takeoff Distance
TOFL	Takeoff Field Length
TOGW	Takeoff Gross Weight
TRL	Technical Readiness Level
WACC	Weighted Average Cost of Capital

BOEING

CONTENTS

1.0 INTRODUCTION

Wing sizing for current transonic transport aircraft represent trades between efficient cruise and effective high-lift characteristics. This includes trades of weight, complexity, supportability, realiability, and noise induced by complex high lift systems against wing planform sizing for cruise around maximum lift-to-drag ratio. Most of these trades lead to high-lift systems that combine leading edge devices (e.g., slats, Krueger flaps) with slotted single- or multi-element trailing edge flaps.

McLean et al. [1] explored a range of active flow control (AFC) applications for improving the efficiency of next-generation commercial transonic transport aircraft. They identified AFC-enhanced simplified high-lift systems as a high payoff / high risk technology for significantly reducing weight and fuel consumption for the targeted aircraft class. The rationale was that AFC would remedy flow separations that are anticipated when current high-lift systems would be replaced with mechanically simpler and lighter variants with simply hinged single element trailing edge flaps.

Since that McLean report, much research has been directed at exploring the capabilities and limitations of AFC applications to simplifed high lift systems, starting with computational and experimental studies on two-dimensional airfoils [2] and some exploratory applications to non-conventional configurations such as the AFRL Advanced Theater Transport (ATT) [3] and the AFRL Speed Agile [4] concepts that were enabled only through AFC applications.

The encouraging findings in these studies on AFC-enhanced high-lift concepts motivated the current trade study which aims at exploring the feasibility of using AFC for achieving lighter and mechanically simpler high-lift systems for transonic commercial transport aircraft. This assessment was conducted in four steps. First, two baseline high-lift concepts were developed with one being representative of current high-lift wing designs and the other being a mechanically simplified high-lift configuration for AFC integration. In the next step, the high-lift aerodynamics of these two high-lift CRM variants were assessed using Computational Fluid Dynamics (CFD) solutions to the Reynolds-Averaged Navier-Stokes (RANS) equations for steady flow. These CFD assessments identified the high-lift performance that needs to be recovered through AFC to have the CRM variant with the lighter and mechanically simpler high-lift system match the performance of the conventional high-lift CRM.

The thus-established AFC aerodynamic performance targets guided conceptual design integration studies for the AFC-enhanced high-lift systems on a reference configuration. This project element aims at the identification of suitable AFC/airframe integration concepts that match take-off and landing approach capabilities of current fleet transonic transport aircraft while yielding weight and fuel savings that translate into a positive net present value (NPV).

At the conclusion of the current study, which is rather exploratory in nature, technical challenges of AFC-enabled high-lift systems for modern transonic commercial transports were to be identified for future technology maturation efforts.

2.0 CONVENTIONAL AND AFC-ENABLED HIGH LIFT SYSTEM DEVELOPMENT

Prediction of high-lift characteristics has long been known to challenge the capabilities of CFD-based flow solvers. A good survey of the state of the art in CFD-based high-lift analysis can be found in the report on the latest AIAA high-lift prediction workshop [5]. The baseline

configuration for this series of AIAA workshops is the so-called DLR-F11 configuration (see Fig.1). After having given some serious consideration to adopting this reference geometry for the present study, it was decided to proceed instead with the development of a high-lift variant of the public-domain Common Research Model (CRM) [6], also shown in Figure 1. Developing a high-lift variant of the CRM configuration avoids drawbacks associated with the DLR-F11 model such as a non-functional integration of leading-edge and trailing-edge high lift devices, lack of tail and landing gear definition, and limited access to wind-tunnel test data.

2.1 Conventional High-Lift CRM Configuration

The CRM configuration is representative of a twin-aisle transonic civil transport aircraft which was designed only for a single transonic cruise condition. The static aeroelastic effects at a nominal cruise condition are accounted for by defining a wing shape showing the effects of aerodynamic loads rather than adopting its jig shape. To facilitate the aerodynamic design of a representative conventional high-lift wing design, the CRM wing was re-sheared to allow for a linear slat trailing edge while retaining total wing dihedral. (Figure 2).

In a planform view, Figure 3 shows the layout of the leading-edge slats and the trailing-edge single element flaps with Fowler motion. The arrangement and the geometric dimensions (e.g., chord ratios, span extents of the flaps) were chosen from a survey of current production civil transport aircraft. This is illustrated in Figure 4 which shows planform views for a cross section of current fleet transonic transport aircraft along with an indication of the type of leading-edge (LE) and trailing-edge (TE) devices employed. From studying Figure 4, it appears that the trend in current fleet aircraft is toward high lift systems that combine slats with single-element slotted flaps with Fowler motion. Hence, this layout was selected for developing the high lift variant of the CRM configuration.

The planform views in Figure 4 also guided the selection of the span extents of the slats and trailing edge flaps. The slat and trailing edge flap chord ratios in Figure 3 were chosen to be in family with those for the current fleet aircraft listed in Figure 4. Here, ‘in family’ means that they were chosen to roughly fall in the middle of the bands of the leading-edge and trailing-edge device chord ratios shown in Figures 5 and 6.

Likewise, the range of the Fowler motion of the slotted trailing edge flaps of the conventional high-lift CRM was also chosen to be in family with the chord ratios defined by the distance between spoiler trailing edge and flap trailing edge for the fleet aircraft used to build the plot in Figure 7.

2.2 Simplified High-Lift CRM Configuration

The intent of defining a simplified high-lift CRM configuration is to reduce weight, part count, and excrescence drag due to any fairings needed to aerodynamically dress the mechanical systems for operating the high-lift devices, particularly, the slotted trailing edge flaps with Fowler motion. In that vein, a simply hinged trailing edge flap is the simplest possible trailing edge device for increasing wing camber. Allowing for a slotted flap configuration maintains the mechanical simplicity of the simply hinged trailing edge flap while making for aerodynamically more effective designs.

To protect against premature stall, these two types of trailing edge high-lift devices need to be paired with a leading edge device. One choice is a Krueger flap design for which some mechanically rather simple designs are available. A drooped leading edge is mechanically still sim-

pler than a slat while avoiding the careful rigging required for an effective slat installation. While both Krueger flaps and drooped leading edge designs are found on current fleet aircraft, morphing leading edges are sitting at low technical readiness levels (TRLs) but hold the promise of being simpler while being as effective aerodynamically if not more so than either of the other two leading edge device concepts.

The permutation of any of these five high-lift device concepts gives the matrix of six possible high-lift design concepts shown in Table 1. To accommodate resource and schedule constraints, a Quality Function Deployment (QFD) approach was adopted to identify the preferred simplified high lift concept among the options shown in Table 1. The QFD approach employed in this study is illustrated in Figure 8. On the left-hand side of the House-of-Quality in Figure 8, the programmatic requirements are listed. As they were provided by NASA, they are being referred to as "NASA Requirements." Along the ceiling underneath the pitched roof, a set of derived requirements is spelled out. They are referred to as technical requirements that a design must meet to achieve the system or programmatic requirements. For each technical requirement, a QFD score is assigned. Adopting the nonlinear scale commonly used in QFD assessments, the ratings are in powers of three (i.e., 1 for low importance, 3 for intermediate importance, and 9 for high importance). A weight is applied to each QFD score, reflecting NASA's prioritization of their system performance requirements. Summation of the weighted technical requirement scores gives a technical priority score.

	LE Devices		
TE Devices	**Krueger**	**Drooped LE**	**Morphing LE**
Simply-Hinged Flap	●	●	●
Slotted TE Flap (no Fowler motion)	●	●	●

Table 1 All six simplified high-lift systems in this study aim for reductions in weight, part count, and excrescence drag.

In the basement of the House of Quality, the six possible combinations of leading-edge and trailing-edge high lift devices are listed as 'concepts.' A score is assigned to each 'concept' in each technical requirement. These score reflect grading on a curve with '1' being the lowest and '5' being the highest score. The total score for each high-lift concept is computed from summing up each concept score, scaled with its technical priority score. This QFD approach identifies a preferred simplified high-lift CRM concept that features drooped leading edge devices and simply hinged trailing edge flaps.

The pitched roof of the House of Quality permits taking into account synergistic or canceling interactions of any two or more particular technical requirements. This option was not exercised in the present study. This additional evaluation dimension is considered to add a layer of refinement that seemed out of line with the rough order of magnitude estimation approach adopted here to identify a preferred simplified high lift CRM system.

For the same wing planform shown in Figure3, Figure 9 shows the layout of the simplified high-lift CRM wing. The chord ratio and span extents of the drooped leading edge devices are close to that of the slats of its conventional high-lift CRM sibling, as are chord ratios and span extents for the conventional and the simplified trailing edge flaps. This similarity in planform layout for both simplified and conventional high-lift wing concepts aims to minimize the impact of any geometric differences on the high-lift aerodynamics.

Note that the simply hinged flap will require a spoiler design different from that adopted for the conventional high-lift design. In absence of a Fowler motion capability, the trailing edge of the spoiler for the simplified high-lift system has to lie upstream of the leading edge of the simply hinged trailing edge flap.

3.0 CFD-BASED ASSESSMENTS OF HIGH-LIFT AERODYNAMICS

3.1 Setup of CFD Analyses

A series of overset grids was built to model the various high lift CRM configurations. Surface grid generation was accomplished using a Boeing-developed program called MADCAP. Building of the volume grids and establishing connectivity for zone-to-zone communication relied on NASA tolls such as Chimera Grid Tools and Pegasus5. Table 2 summarizes the grids employed in the present high-lift performance assessments. There were grids for the CRM wing/body and wing/body/nacelle/pylon configurations. The former configuration was gridded for takeoff and landing approach configurations, at wind-tunnel (i.e., 'low' Reynolds number) and fight conditions (i.e., 'high' Reynolds number). The number of grids points used varied with complexity of the configuration and with the freestream condition (i.e., wind-tunnel and flight conditions). As for the latter, care was taken to resolve the viscous sublayer by using a grid spacing of $y^+=1$ along and normal to solid walls.

Case Description	Nacelle/ Pylon	# of Zones	# of Points
Conventional, landing, low/high RN	On	61	62.9 million
Conventional, landing/takeoff, high RN	Off	38	52.2 million
Conventional, landing/takeoff, low RN	Off	38	48.8 million
Simplified, landing, high RN	Off	20	36.7 million
Simplified, landing, low RN	Off	20	33.7 million
Simplified, takeoff, high RN	Off	18	36.4 million
Simplified, takeoff, low RN	Off	18	33.5 million

Table 2 Listing of all computational grids utilized in CFD-based assessment of CRM high-lift aerodynamics.

All computations were carried out with the OVERFLOW flow solver. This is a Reynolds Averaged Navier-Stokes (RANS) code widely used to compute subsonic, transonic, and supersonic flow over complex configurations. This node-centered flow solver is designed for structured overset grids systems like those built for this high-lift CRM study. The OVERFLOW solution system can be run in many modes. Those employed for the present analyses are summarized as follows

- Code version 2.2g
- Spalart Allmaras turbulence model with curvature correction (SA-RC)
- Flux-difference splitting for right hand side (RHS) of discretized RANS equations
- Central differencing for left hand side (LHS) of discretized RANS equations

- Low-Mach number preconditioning for mitigating stiffness of compressible discretized RANS equations at low-speed freestream conditions

All cases were run with the assumption of fully developed boundary layers (i.e., without laminar/turbulent transition modeling). For computations for flight conditions, the Reynolds number was 24.6 million, corresponding to a freestream Mach number of 0.2 at an altitude of 10,000 ft. For computations at wind-tunnel conditions, the Reynolds number was set at 3.3 million based on an assumed model scale of 10%, sea-level conditions, and a freestream Mach number of 0.2.

The geometric parameters used for computing all force and moment coefficients are summarized as follows:

- C_{ref} = 275.8 in (MAC)
- $S_{ref}/2$ = 297,360.0 in^2
- b/2 = 1156.75 in
- X_{ref} = 1325.9 in, Y_{ref} = 0.0 in, Z_{ref} = 177.95 in

High-Lift CRM OVERFLOW Runs - *CONVENTIONAL*

Series	Run	Priority	Horiz Tail	Nacelle / Pylon	LE Deflection (deg)		TE Deflection (deg)		Reynolds No.	Altitude	Temp				Alph
					IB Slat	OB Slat	IB Flap	OB Flap		(ft)	(deg R)	Re/in	Re_{mac}	Mach	Flag
Clean Wing: High Speed Loft (original geometry from DPW-IV)															
1	1	2	off	on	retracted	retracted	retracted	retracted	flight	10,000	483.01	89268.3	24,620,197	0.20	A5
1	2	2	off	off	retracted	retracted	retracted	retracted	flight	10,000	483.01	89268.3	24,620,197	0.20	A5
Clean Wing: Low Speed Loft (re-sheared for straight slat TE)															
2	1	2	off	on	retracted	retracted	retracted	retracted	flight	10,000	483.01	89268.3	24,620,197	0.20	A1
2	2	2	off	on	retracted	retracted	retracted	retracted	flight	10,000	483.01	89268.3	24,620,197	0.20	A2
2	3	2	off	on	retracted	retracted	retracted	retracted	WT	sea level	518.67	11834.5	3,263,955	0.20	A1
2	4	2	off	on	retracted	retracted	retracted	retracted	WT	sea level	518.67	11834.5	3,263,955	0.20	A2
2	5	2	off	off	retracted	retracted	retracted	retracted	Flight	10,000	483.01	89268.3	24,620,197	0.20	A5
Landing															
3	1	1	off	on	12.5	45	30	30	WT	sea level	518.67	11834.5	3,263,955	0.20	A3
3	2	1	off	on	12.5	35	30	30	WT	sea level	518.67	11834.5	3,263,955	0.20	A4
3	3	1	off	on	12.5	25	30	30	WT	sea level	518.67	11834.5	3,263,955	0.20	A4
3	4	1	off	on	12.5	45	30	30	Flight	10,000	483.01	89268.3	24,620,197	0.20	A3
3	5	1	off	off	12.5	25	30	30	WT	sea level	518.67	11834.5	3,263,955	0.20	A3
3	6	1	off	off	18	25	30	30	WT	sea level	518.67	11834.5	3,263,955	0.20	A3
3	7	1	off	off	18	25	30	30	Flight	10,000	483.01	89268.3	24,620,197	0.20	A3
Takeoff															
4	1	3	off	off	18	25	15	15	WT	sea level	518.67	11834.5	3,263,955	0.20	A3
4	2	3	off	off	18	25	15	15	Flight	10,000	483.01	89268.3	24,620,197	0.20	A3

Alpha Flags
A1: α = 0 to 20 deg in 4 deg increments
A2: α = 11, 13 deg
A3: α = 0, 4, 8, 12, 13, 14, 15, 16, 18, 19, 20, 21 deg
A4: α = 12, 15, 18, 19, 20, 21 deg
A5: α = 4, 8, 12, 13, 14 deg

Table 3 Run Matrix for the conventional high-lift CRM configuration with angle-of-attack schedules.

3.2 CFD Run Matrices

Tables 3 and 4 provide the run matrices for all CFD analyses including angle-of-attack schedules. As summarized in Table 3, for the conventional high-lift CRM configuration, 157 flow field solutions were computed for 10 configurations including nacelle/pylon on or off, clean wing set up(i.e., all leading-edge and trailing-edge devices are assumed in a fully retracted position), and landing and takeoff configurations with different slat and trailing edge flap settings.

There are 55 solutions for the clean wing setting, 80 solutions for landing and 22 solutions for takeoff configurations.

As summarized in Table 4, for the so-called simplified high-lift CRM configuration, 52 flow field solutions were computed for four wing/body configurations in landing and takeoff configurations with different dropped leading edge and trailing edge flap settings. There are 30 solutions for landing and 22 solutions for takeoff configurations.

High-Lift CRM OVERFLOW Runs - *SIMPLIFIED*

Series	Run	Priority	Horiz Tail	Nac / Pyl	LE Droop (deg) IB Slat	LE Droop (deg) OB Slat	TE Droop (deg) IB Flap	TE Droop (deg) OB Flap	Reynolds No.	Altitude (ft)	Temp (deg R)	Re/in	Re_{mac}	Mach	Alpha Flag
Landing															
1	1	1	off	off	20	25	30	34	WT	sea level	518.7	11835	3,263,955	0.20	A0
1	2	1	off	off	20	25	30	34	Flight	10,000	483.0	89268	24,620,197	0.20	A0
1	3	1	off	off	0	0	30	34	WT	sea level	518.7	11835	3,263,955	0.20	A0
1	4	1	off	off	10	15	30	34	WT	sea level	518.7	11835	3,263,955	0.20	A0
Takeoff															
2	1	2	off	off	20	25	15	17	WT	sea level	518.7	11835	3,263,955	0.20	A0
2	2	2	off	off	20	25	15	17	Flight	10,000	483.0	89268	24,620,197	0.20	A0

Alpha Flag
A0: α = 0, 4, 8, 12, 13, 14, 15, 16, 18, 19, 20, 21 deg

Table 4 Run matrix for the simplified high-lift CRM configuration with angle-of-attack schedules.

3.3 CFD Results for Wing/Body/Nacelle/Pylon Configurations

Figure 10 shows the variation of lift coefficient with angle-of-attack for a clean-wing/body/nacelle/pylon configuration at freestream flight conditions. At 12 degrees angle of attack, a glitch in the lift curve is observed. This phenomenon is explained with the lift-versus/pitching moment plot along with wing surface flow visualizations in Figure 11. The initial kink in the lift/pitching-moment curve is associated with an angle of attack of 12 degrees. Comparing wing surface flow plots at angles of attack of 12 and 13 degrees indicate that separated flow from the nacelle is swept over the wing, causing the wing flow to separate as well downstream of the installed nacelle. The second kink in the lift-versus/pitching moment plot is associated with the onset of outboard wing stall. This is inconsistent with established high-lift design practice that aims to have the inboard wing sections stall first to maintain roll control.

To pinpoint the root causes for these undesirable flow separation characteristics, the conventional wing/body/nacelle/pylon configuration was re-run in a landing approach configuration at both wind-tunnel and flight conditions. The results for these runs are summarized in Figure 12. Figure 12 shows the variation of lift with angle-of-attack for a clean and a landing configuration, and surface flow visualizations in top views for maximum and post-stall conditions. As expected, lift increases with higher freestream Reynolds number as the Navier-Stokes solutions comes closer to the optimum inviscid flow solution as the Reynolds number is raised. The benefits of increased camber (i.e., shift in lift curve slope) and improved stall protection due to the deployed slats (i.e., increase install angle of attack) are obvious. For the landing configuration, one would expect higher values for maximum lift and the associated angle of attack based on the performance of current fleet aircraft which the conventional high-lift CRM configuration was intended to be representative for. This can be understood by inspection of the surface flow images. At maximum lift, a rapid growth of the region of separated flow across the mid-wing section id observed due to a poor nacelle/wing integration at maximum and immediate post-stall

conditions. Note that both surface flow images indicate stalled flow over the outboard wing section. It appears that while this is undesirable from an aircraft control perspective, it is of secondary importance to maximum lift performance.

In view of the results in Figure 12, a decision had to be made whether to improve the nacelle/pylon/wing integration or to bypass this issue by reverting to wing/body-only CFD analysis. Considering resource and schedule constraints, the decision was made to process with the CFD analysis for wing/body high-lift CRM configurations.

3.4 CFD Results for Wing/Body Configurations

Figure 13 illustrates the modifications to the conventional and simplified high-lift CRM configurations. The nacelles and pylons have been removed, and a transition element has been designed to fill in the gap between inboard and outboard leading edge devices that was created by removal of the pylon. This transition element introduces some waviness in the leading edge contour due to the differential positioning of the inboard and outboard slats and drooped leading edge settings for the conventional and simplified high-lift CRM configurations, respectively. Figure 13 also shows the difference in trailing edge flap settings for the conventional and simplified high-lift designs. For the conventional high-lift CRM configuration, the trailing edge flaps is deflected down and moved aft, creating a slot between main wing and flap. For the simplified high-lift CRM concept, the trailing edge flap is deflected down only without any slot-creating Fowler motion.

Figure 14 shows the variation of lift coefficient with angle of attack for the conventional CRM configuration with and without nacelle/pylon installations. Results for several slat settings are shown, all computed at wind-tunnel freestream conditions. Without the sub-optimal nacelle/wing installation, maximum lift increases by about five percent and the associated angle of attack by about a couple degrees. One could say that the trends were to be expected, but that the magnitude of the high-lift improvements are still falling short of expectations for a high-lift design intended to be representative of the high-lift performance of current fleet transonic transport aircraft. As illustrated by the surface flow visualization inserts, this shortfall is due to the premature stalling of the outboard wing sections. If anything, these non-representative wing stall characteristics appear to be exacerbated by the high-lift system when compared to the stall characteristics of the clean wing configuration (see Figure 10). This shortfall in maximum lift performance is expected to be cured by re-twisting and re-cambering the CRM wing which turns out to be a point design for transonic cruise only.

Figures 15 and 16 compare lift performance for the clean wing configuration with those for the conventional and simplified high-lift CRM configurations. Figure 15 shows these comparisons for the respective high-lift CRM concepts for a landing-approach rigging, and Figure 16 repeats these comparisons for takeoff settings. As before, lift increases for any give angle of attack when going from wind-tunnel to flight freestream conditions. As also is to be expected, the computed lift values for the simplified high-lift CRM configuration fall somewhere between those for the clean and the conventional high-lift CRM configurations.

While Figure 14 has already addressed the sensitivity of the high-lift performance of the conventional high-lift CRM concept to slat settings, the computed lift variations with angle of attack in Figure 17 show that the drooped leading edge setting for the simplified high-lift CRM concept

that was used for the comparisons in Figure 15 and 16 is close to one producing optimum high-lift performance.

3.5 Performance Targets for AFC-Enhancements to Simplified High-Lift CRM Concepts

The purpose of the CFD-based high-lift assessments for the conventional and simplified high-lift CRM concepts is to quantify the decrements in high-lift performance for the simplified high-lift system that need to be recovered by the integration of AFC. Figure 18 compares the variation of incremental lift with angle of attack for the conventional and the simplified high-lift CRM wing/body concepts at wind-tunnel and flight freestream conditions. For any given angle of attack, the largest loss in lift is observed for the landing configurations at low Reynolds number (i.e., wind-tunnel) conditions. Note that these comparisons are for untrimmed lift conditions. Figures 19 and 20 help to assess the effect of trim on these lift decrements.

Figures 19 and 20 compare pitching moments for the clean wing configuration with those for the conventional and simplified high-lift CRM wing/body configurations. Figure 19 shows these comparisons for the respective high-lift CRM concepts for a landing-approach rigging, and Figure 20 repeats these comparisons for takeoff settings. In general, the Reynolds number effects manifest themselves by yielding higher pitching moment values for any given lift value when going from wind-tunnel to flight freestream conditions. The same observations hold true when comparing lift for any given pitching moment when going from wind-tunnel to flight freestream conditions.

From Figures 19 and 20, it appears that the conventional high-lift CRM wing/body concept produces more nose-down pitching moment than the simplified CRM wing/body concept. This, in turn, requires more download from the horizontal tail for the conventional than for the simplified high-lift CRM concept. This tail download will reduce lift for the trimmed conventional high-lift CRM concept. In other words, the lift decrements shown in Figure 18 that need to be recovered through AFC deployment are conservative. They should be expected to be reduced for trimmed full CRM concepts (i.e., wing/body/nacelle/tail configurations).

4.0 AFC SIZING

Several AFC concepts have been explored over the years. Prevalent among them are pneumatic and synthetic AFC actuators. To take advantage of the data obtained in a NASA/Boeing wind-tunnel test of an AFC-enhanced full-scale Boeing-757 vertical tail at the National Full Scale Aerodynamic Complex (NFAC), the decision was made to consider pneumatic AFC actuators for recovering the high-lift performance of the simplified high-lift CRM wing/body concept to match that of its conventional high-lift counterpart. It should be noted here that public-domain documentation of this NFAC AFC wind-tunnel test is forthcoming but not in hand yet.

The AFC augmentation for the simplified high-lift CRM concept needs to be sized to match the performance of the conventional high-lift CRM at both landing-approach and takeoff conditions. There is some debate as to the ability of CFD to reliably predict the stall characteristics of high-lift transport configurations. To avoid having the present AFC sizing exercise contaminated by potentially contentious Navier-Stokes solutions at stall, so-called nominal landing-approach and takeoff conditions have been selected for estimating AFC requirements for a simplified high-lift CRM concept.

Figure 21 compares computed surface pressures for the conventional and the simplified high-lift CRM configurations along with offbody iso-surfaces that indicate the enveloped of separated flow. The iso-surfaces represent the location of off-surface flow with a zero axial velocity component. It can be seen that the both trailing-edge flaps of the simplified high-lift CRM are fully separated. This is the prime contributor to the loss of high-lift performance of the simplified high-lift CRM compared to its CRM counterpart with the conventional high-lift system. This comparison is illustrated in Figure 21 for a so-called nominal landing condition where the approach speed is large than 123% of the stall speed. The comparisons of lift variation with angle of attack in Figure 21 show that the so-called nominal approach condition occurs well within the linear range of the lift curves with a safe margin against maximum-lift or stall conditions.

The lift curves in Figure 21 are plotted for wind-tunnel and flight freestream conditions. To quantify the lift that needs to be recovered with AFC, first locate the intercept between the lines indicating nominal lift coefficient with the lift curve for the conventional high-lift CRM concept. The difference in lift between the simplified and conventional high-lift CRM concept at the angle-of-attack associated with this intercept gives the lift that needs to be recovered by AFC. Applying this process at flight freestream conditions shows that the AFC performance needs to recover about 18% of the lift decrement to produce matching lift for both simplified and conventional CRM high-lift systems. Repeating this process for the lift traces computed at wind-tunnel freestream conditions indicates that lift decrement to be 30% going from the conventional to the simplified CRM high-lift system.

For a nominal takeoff condition (i.e., take off speed is greater than 113% of the stall speed), Figure 22 shows the variation of lift with angle of attack and the variation of lift with lift-to-drag ratio. The latter is important as the lift-to-drag ratio at takeoff is an important driver in the mission performance of commercial transport aircraft, as will be shown later in the net present value (NPV) analysis section. As before in the comparisons in Figure 21, choosing a nominal takeoff condition ensures that the AFC estimates are computed for the linear segments in the lift curves separated from stall conditions by a robust margin.

Applying the same analysis process as used with Figure 21, it turns out that AFC needs to recover about 15% in lift decrement at both wind-tunnel and flight freestream conditions to produce matching lift for both simplified and conventional high-lift systems. In addition, for takeoff, this needs to happen while maintaining the lift-to-drag ratio to avoid adverse impact of an AFC integration on the overall mission performance of an AFC-enhanced simplified high-lift CRM concept.

In surveying the lift decrements at landing-approach and takeoff conditions due to the mechanical simplification of the CRM high-lift system, it appears that an AFC sizing at wind-tunnel freestream conditions overall is more challenging than at flight freestream conditions. To produce conservative AFC estimates, the decision was made to size AFC at wind-tunnel freestream conditions.

4.1 Inviscid Performance Limit Concept for AFC Sizing

Previous studies have shown that optimum AFC sizing can be characterized as recovering in the limit inviscid flow which by definition is free of flow separation. Sizing AFC in excess of this so-called inviscid limit, flow control turns into circulation control which is still an effective while no longer the most efficient means of flow control. This is illustrated Figure 23. This fig-

ure shows the variation of side force with momentum of the AFC discharge for the aforementioned Boeing-757 vertical tail. Without AFC, the flow over the deflected rudder is separated. With an AFC discharge of a specific momentum of about 0.11, the flow over the deflected rudder remains attached and produces a sideforce equal to that computed from an Euler solution for inviscid flow over the same Boeing-757 vertical tail configuration. If the specific momentum of the AFC discharge is further increased beyond 0.11, the slope of the side force trace drops significantly, becoming typical of side force sensitivities found in circulation control setups.

Applying these lessons learned from the Boeing-757 AFC sizing, first inviscid limit solutions were computed from Euler solutions for flow over the simplified high-lift CM configuration with dropped leading edges and trailing edge flaps at landing approach settings. The next step involves Navier-Stokes solutions over the same simplified high-loft CRM configuration where the AFC discharge was simulated by applying constant blowing boundary conditions. These AFC mass flow boundary conditions prescribe total pressure and direction of the velocity vector along strips just upstream of the trailing edge flaps.

4.2 CFD-Based AFC Sizing

Figure 24 summarizes the results from these initial AFC sizing estimates. This composite figure shows variation of lift with AFC mass flow in the right upper quadrant. This plot also gives the lift level of the conventional high-lift CRM configuration. This is the target lift level that needs to be recovered by AFC deployment. In addition the inviscid lift limit is indicated as well. Any AFC solution where the achieve lift exceeds this inviscid limit indicates that the dialed-in AFC mass flow coefficient is too high producing a blend of AFC and circulation control.

The plot in the lower right quadrant in Figure 24 shows spanload distributions. To maintain the lift-to-drag ratio of the conventional high-lift CRM configuration, AFC needs to be sized to resemble the spanload distribution of that conventional high-lift CRM configuration. Also in Figure 24 are three plots that give the computed surface pressures and iso-surfaces that indicate separated flow (see previous discussion of similar plot layouts for Figure 21). These flow visualizations correlate with the data points in the Cl-vs-Cq plot in the right upper quadrant. AFC applied to both inboard and outboard trailing flaps is twice as effective as AFC application to the inboard trailing-edge flap only. Subsequently the AFC mass flow over the outboard trailing-edge flap was reduced to more closely match the spanload distribution (i.e., the L/D ratio) of the conventional high-lift CRM configuration.

This initial step in the current CFD-based AFC sizing process was followed up with a more detailed AFC model. As shown in Figure 25, backward-facing steps were carved into the upper trailing-edge flaps surfaces. The vertical extend of these steps is scaled from the AFC integration validated in the aforementioned NFAC Boeing-757 AFC test. Along the vertical faces of the backward facing steps, AFC is either modeled as blowing through a continuous strip or as discharge through discrete ports.

The discrete AFC port computer model with 19 ports along the inboard and 18 ports along the outboard flap is illustrated in Figure 26. Each port consists of a set of grids, meaning that the internal port flow is modeled. Trial and error is employed to guide the orientation of the discrete ducts to achieve the desired Coanda effect for energizing the boundary-layer flow over the flaps. An initial nozzle orientation at a steeper angle to the flap surface proved ineffective in re-

attaching the flow over the trailing edge flap. A later iteration with the nozzle cut into the flap surface at a shallower angle proved effective.

Figure 27 adopts a layout similar to that of Figure 24. Whereas the results in Figure 24 were for continuous blowing across slots over the full spanwise extent of both inboard and outboard trailing edge flaps, Figure 27 shows results for a discrete AFC model with constant blowing through a bank of 37 ports. The AFC mass flow rate was dialed in to roughly match the spanload distribution of the conventional high-lift CRM concept. This setup succeeds in simultaneously approximating the takeoff lift-to-drag characteristics of the conventional high-lift CRM concept while recovering its lift. At an aircraft systems level, this AFC setup translates into an air mass flow rate of 72 lbm/sec at an operating pressure of 80 psia for the full wing (i.e., left and right wing halves).

5.0 TRADE STUDY ON AFC-ENABLED SIMPLIFIED HIGH-LIFT SYSTEM

This section discusses results from a system-level trade study on the mechanically simplified high-lift system to accommodate a pneumatic AFC system defined and sized in the preceding section. The purpose of this trade study is to identify any potential weight and fuel savings from the mechanically simplified high-lift system. This requires a baseline transonic transport concept configuration to increment any such potential savings from. In this study, the NASA ERA-0003 concept was chosen to be that baseline concept. The ERA-0003 concept represents a twin-aisle 275-passenger transonic transport aircraft with 1990-era technology projections [7]. Its high lift system was comprised of Krueger flaps and of single-element slotted trailing edge flaps. These features make the ERA-003 concept comparable to one that the CRM OML was defined for. Key dimensions for the ERA-0003 concept are provided along with a 3-view and a cabin layout in Figure 28.

Four different options have been considered for providing the pressurized air mass flow rate of 72 lbm/sec at an operating pressure of 80 psia that the CFD-based AFC estimation calls for:

Option 1: use existing tail-mounted APU

Option 2: install a dedicated APU system

Option 3: siphon off turbine bleed

Option 4: siphon off core bleed

Option 1 is derived from the AFC installation on the recent Boeing-757 NFAC full-scale experiment, where the AFC mass flow rate and operating pressure are consistent with the capability of a Boeing-757 APU. While the CFD-based estimates of the power requirements of the current AFC high-lift application were found to scale well with data from that recent Boeing-757 vertical tail AFC test at NFAC, this also means that the power requirements exceed the capabilities of APU systems that would be typical of commercial transonic transports. This situation gets exacerbated by the fact that one would have to provide for redundancy in case of an APU failure and by the long pressure lines from a tail-mounted APU to the wing-mounted AFC units. These considerations eliminated Option 1 from further consideration.

For option 2, it was assumed that engine core bleed would provide an air mass flow rate of 8 pps at 80 psia. For the two-engine ERA-0003 concept, this means that two dedicated APUs would be required to provide the remaining 56 pps of air mass flow at 80 psia. There are APUs available that would satisfy this requirement. For instance, the Honeywell 331-500 engine seems

to hold the potential for producing 28 pps of air mass flow at the 80 psia after some modifications, such as the removal of its power shaft capability while adding a second stage to the air compressor. Two of these engines would satisfy the AFC high-lift power requirements.

The Honeywell 331-500 engine measures 80” in length, 35” in height, and 48” in width. To minimize pressure line losses, two of these APUs would be installed in the cargo hold close to the wing. Each engine weighs in at about 650 lbs. Their operation would require provisions for inlet (350 sq.in. / unit) and exhaust (200 sq.in / unit) areas. Installation of these dedicated APUs would add further weight due to requirements for engine mounts, firewalls, fire extinguishing gear, controllers, valves, insulation, pre-cooler, and inlet and exhaust apertures with doors. One can easily see that this AFC high-lift design solution combines increases in weight and complexity with likely adverse impact on the configuration aerodynamics due to the dedicated APU inlet and exhaust areas. Hence, option 2 was abandoned as being unlikely to lead to any of the desired aircraft OEW reductions or fuel savings.

The fan bleed design option (i.e., Option 3) is estimated to provide an air mass flow rate of 100 pps, albeit at only 22 psia operating pressure. This alone disqualifies Option 3 from further consideration, apart from the fact that the duct diameter from the engine to the wing would exceed the pylon width and require unconventional propulsion/airframe integration solutions.

The core bleed option (i.e., Option 4) was considered for the system performance study in the remainder of this section. This option is considered to much more readily integrate with the overall ERA-0003 configuration than any of the other alternatives. It also provides the AFC operating pressure that the AFC power estimates call for. The operating pressure is considered more critical than the air mass flow rate for the AFC implementation. Thus, pursuing option 4 implies that further AFC high-lift trade studies can address the mass flow rate requirements (e.g., fewer AFC units or efficiency gains by going to unsteady/intermittent operations rather than continuous blowing).

Figure 29 summarizes the mission performance for the ERA-0003 baseline configuration, and for an un-scaled (center column in Figure 29) and for a re-sized AFC-variant of the ERA-0003 (far right column in Figure 29). The un-scaled AFC variant looks photographically like the baseline ERA-0003, accounts for a lower weight (750 lbs OEW reduction due to AFC) and a reduction in overall drag by 3.3 counts due to elimination of high-lift system fairings. As the core bleed required to feed the AFC system reduces maximum available engine thrust, TOFL increases by about 1,100 ft. The un-scaled AFC variant of the ERA-0003 concept shows a 1.7% gain in range compared to the baseline ERA-0003 design. This is partially due to the increase in fuel which was increased to have both baseline and un-scaled AFC variant of the ERA-0003 take off at the same TOGW. Re-running the performance analysis for same range for both baseline and un-scaled AFC variant of the ERA-0003 indicates fuel savings of 400 gals of fuel for the un-scaled AFC variant.

The re-sized AFC variant of the ERA-0003 increases engine size to make up for the core bleed. The bigger engine and a slightly larger wing recover takeoff performance to match that of the baseline ERA-0003 concept while that overall still yielding mission fuel savings. These results are illustrated in the ‘thumbprints’ in Figures 30 and 31. These plots show lines of constant TOGW, block fuel, rejection field length, optimum altitude, and distance to climb, all plotted against engine thrust (vertical axis) and wing area (horizontal axis). For the baseline ERA-0003 concept in Figure 30, the mission calls for a climb in 200 nm to an initial cruise altitude (ICA) of

35,000 ft. The point where the lowest possible constant fuel burn trace touches the climb-to-ICA boundary sizes the ERA-0003 concept. For the re-sized AFC variant of the ERA-0003 concept in Figure 31, engine thrust and wing area are sized by takeoff field length instead of rate of climb (i.e., thrust and wing area are identified by the point where the lowest possible constant fuel burn trace touches the TOD or takeoff distance constraint).

5.1 Net Present Value (NPV) Assessment

The NPV assessment is carried out for the un-sized AFC variant of the ERA-0003 concept. Flying the same mission as the baseline ERA-0003 concept, its AFC variant is estimated to save 2,595 lbs or 399.2 gals of jet fuel per flight. Assuming an average flight duration of 16 hours per trip and major maintenance intervals of 10,000 flight hours, there are 625 flights between major maintenance stand downs. With 10 major maintenance cycle during an assumed 20-year operational life, the aircraft will complete about 6,000 flights in its lifetime or 300 flights for every year of operation. This translates to lifetime fuel savings of close to 2.4 million gallons of fuel.

The amount of cost savings over the lifetime of an AFC-enabled ERA-000-type aircraft depends on assumptions of fuel price and of a discount rate. The discount rate is a function of the weighted average cost of capital (WACC) of the operator of such an aircraft. The latter directly depends on the capital structure of the operator and its credit rating, and indirectly on macroeconomic factors such as market interest and inflation rates. For the sake of producing an NPV dollar estimate, let the fuel price be assumed at $2/gal on average for the 20-year operational flight, and a discount rate of 10%. This would translate into an NPV of $2.25M per AFC-variant of an ERA-0003-like concept over its 20-year operational life. While this dollar amount might be subject to debate due to the assumption about future fuel prices and operator WACC, the key takeaway here is that the NPV is positive, indicating that there might be value in considering AFC-enabled mechanically simpler high-lift system for an ERA-0003-class aircraft.

6.0 ANALYSIS, CONCLUSIONS, AND RECOMMENDATIONS

The key findings of the current trade study on AFC-enhanced mechanically simplified high-lift systems for commercial transports indicate platform performance improvements due to OEW savings (primarily due to the elimination of the mechanical systems facilitating the Fowler motion of the trailing-edge slotted flaps) and improved aerodynamics (i.e., elimination of high-lift systems fairings). These platform performance improvements translate into a positive NPV, indicating value to an operator to acquire such AFC-enhanced transport aircraft, although the actual NPV amount might be subject to debate.

These key findings hinge on the assumption that further AFC integration studies will identify options for significant reductions in the current AFC power requirements. First pass CFD-based AFC power estimates call for an air mass flow rate of 72 pps at an operating pressure of 80 psia, whereas core bleed from Boeing-777-type 1990's-era turbofan engines provides an air mass flow rate of about 8 pps per engine at an operating pressure of 80 psia. This suggests an AFC performance improvement by a factor of four. In reality, the improvement targets need to be much more stringent, as the indicated core bleed of 8 pps mass flow at 80 psia requires running the engines at full throttle which is impractical during landing approach.

Several potential options have been identified for reducing the AFC air mass flow rate requirements. First off, the high-lift device setting schedules have thus far been adopted from con-

ventional high-lift systems. They might have to be adjusted for AFC-enabled mechanically simplified high lift systems. Secondly, sensitivities of the AFC unit placements such as spacing of AFC units and the alignment of AFC jets with wing surface flow need to be better understood. Thus far only pneumatic AFC units with constant blowing capability have been considered. There might be gains in efficiency by going to sweeping jet-type AFC units or adopting different AFC technologies such as piezoelectric instead of pneumatic AFC units. Finally, the Reynolds number effects need to be better understood as it appears that they are immaterial for takeoff conditions yet relevant for landing-approach operations.

The results of the current AFC high-lift trade study are also somewhat clouded by CRM high-lift characteristics that are non-representative of current high-lift design practices. It is recommended to reintegrate the nacelle/pylon assembly with the CRM wing/body geometry to eliminate any premature flow separation in the mid-span section with the attendant loss in maximum lit capability. In addition, the CRM out wing section ought to be re-cambered and re-twisted to move the onset of wing stall toward the inboard section.

Once the high-lift baseline CRM configuration has been revised, and a suitable AFC integration for high-lift applications has been identified, future studies on AFC-enhanced simplified high-lift systems should shift their focus on validating this technology in large-scale wind-tunnel tests, followed by flight tests to make this technology ready for integration with future transport-type aircraft.

7.0 REFERENCES

[1] McLean, J.D., Crouch, J.D., Stoner, R.C., Sakarai, S., Seidel, G.E., Feifel, W.M., and Rush, H.M., “Study of the Application of Separation Control by Unsteady Excitation to Civil Transport Aircraft, NASA Contractor Report, NASA-CR-1999-209338, June 1999.

[2] DeSalve, M., Whalen, E., and Glezer, A.,”High-Lift Enhancement Using Active Flow Control,” AIAA Paper 2012-3245, June 2012.

[3] Kiedaisch, J., Demanett, B., and Nagib, H., “Active Flow Control Applied to High-Lift Airfoils Utilizing Simple Flaps,” AIAA Paper 2006-2856, June 2006.

[4] Harrison, N.A., Vassberg, J.C., DeHaan, M.A., and Gea, L.-M., “The Design and Test of a Swept Wing Upper Surface Blowing (USB) Concept, AIAA Paper 2013-1102, January 2013.

[5] Rumsey, C.L., and Slotnick, J.P., “Overview and Summary of the Second AIAA High Lift Prediction Workshop, AIAA Paper 2014-0747, January 2014.

[6] Vassberg, J.C., “Introduction: Drag Prediction Workshop,” Journal of Aircraft, Vol. 45, No. 3, May – June 2008, p. 737.

[7] Bonet, J. T., Schellenger, H. G., Rawdon, B. K., Elmer, K. R., Wakayama, S. R., Brown, D., and Guo, Y. P., “Environmentally Responsible Aviation (ERA) Project – N+2 Advanced Vehicle Concepts Study and Conceptual Design of Subscale Test Vehicle (STV),” NASA Contract Report 2013-216519, 2013

8.0 FIGURES

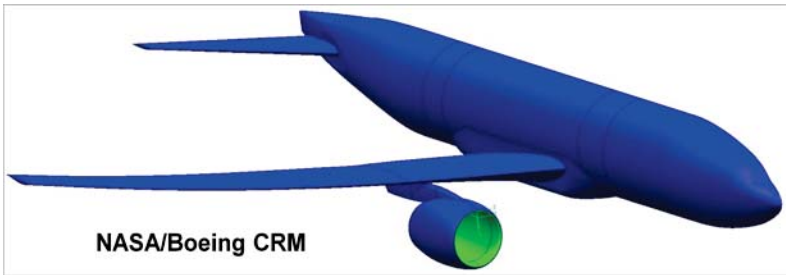

Figure 1 NASA/Boeing Common Research Model (CRM) configuration was chosen over DRL-F11 concept for developing a public-domain high-lift research concept.

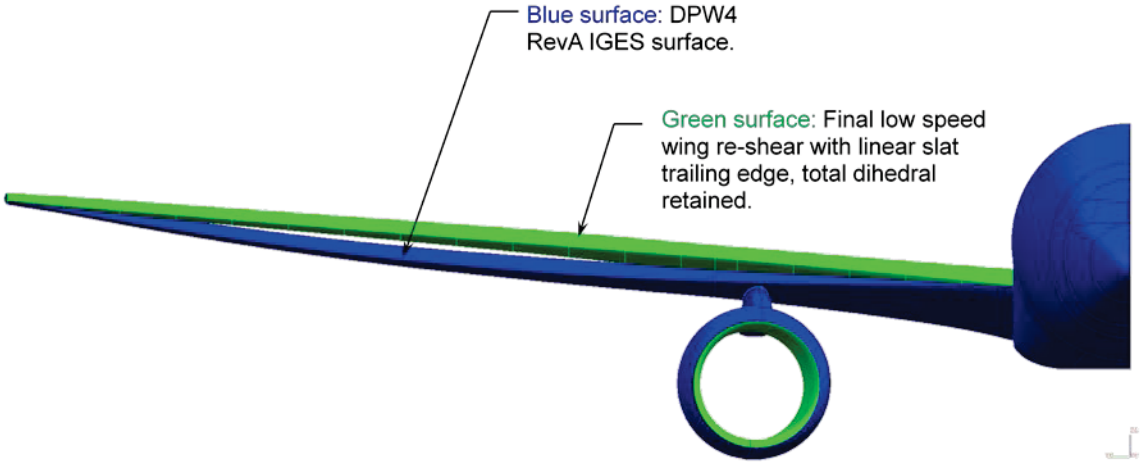

Figure 2 NASA/Boeing Common Research Model (CRM) configuration cruise wing loft was re-sheared for high lift system development.

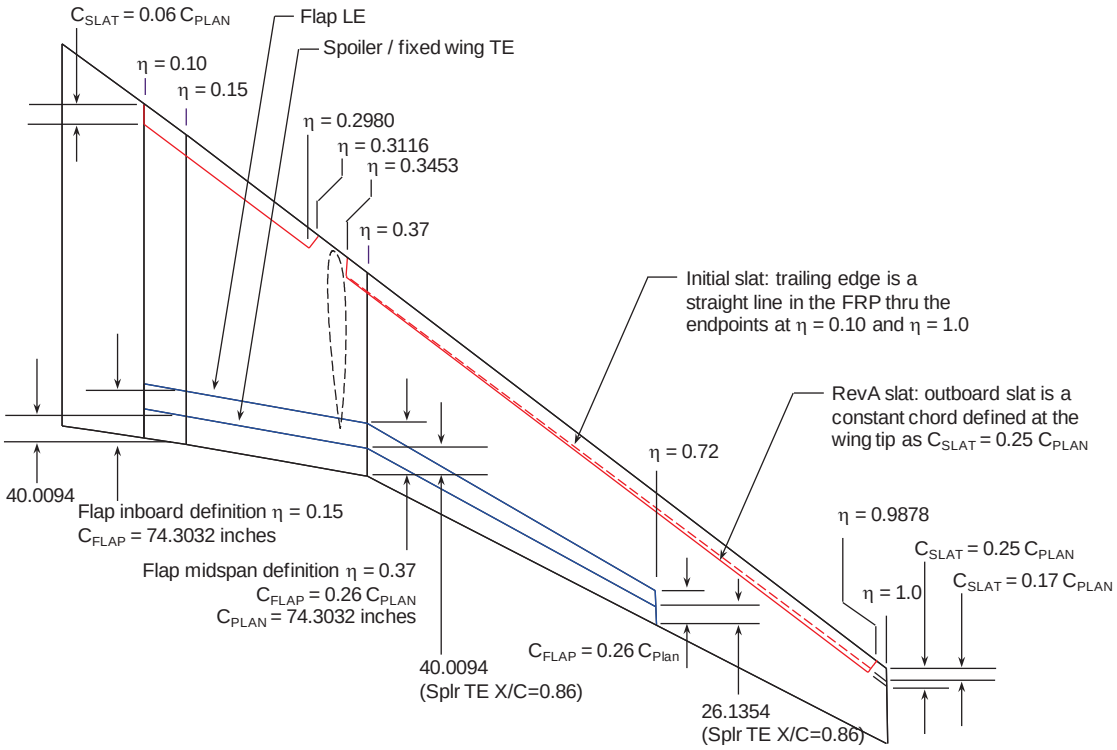

Figure 3 Conventional high lift CRM planform layout is representative of current fleet commercial transport aircraft.

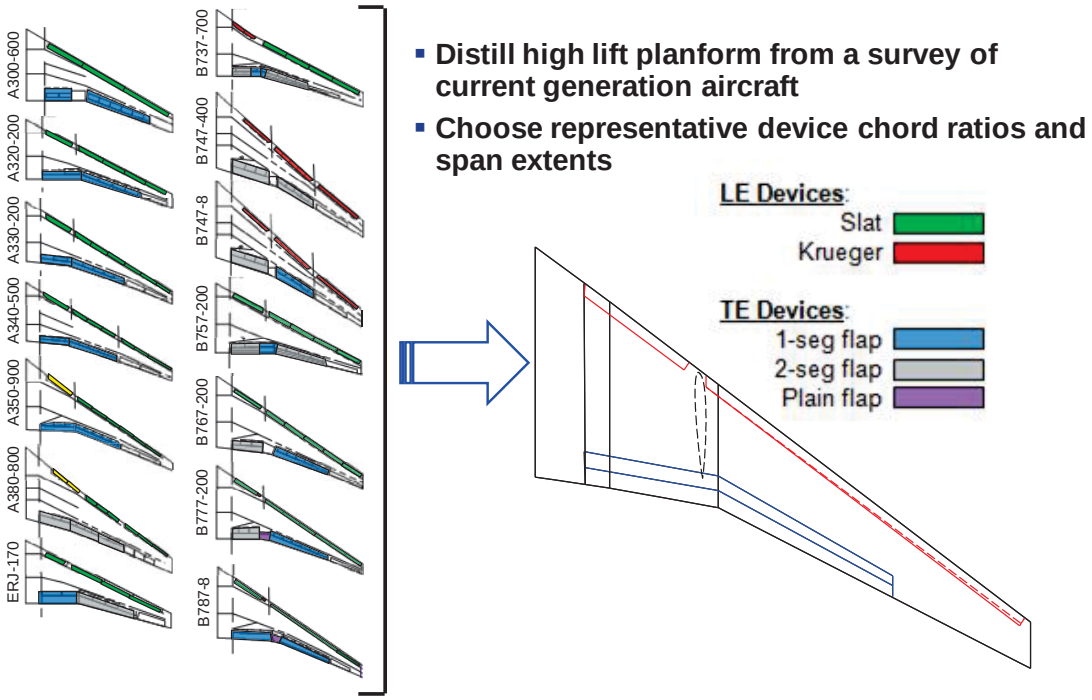

Figure 4 High-lift systems on current fleet aircraft trend toward combining slats with single-element slotted flaps.

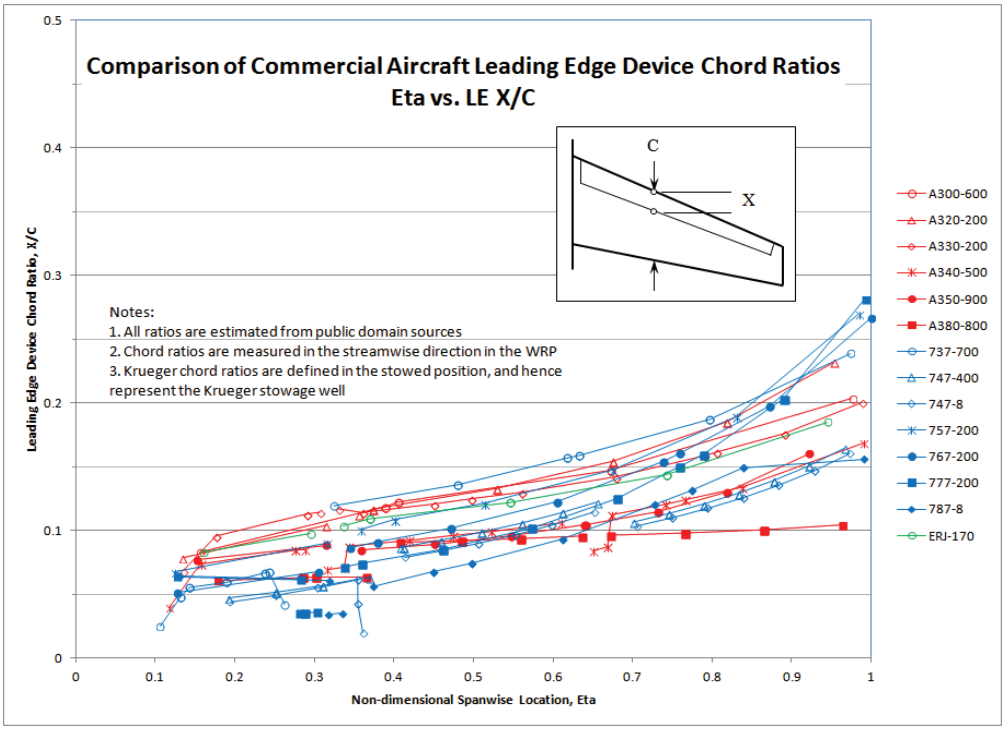

Figure 5 CRM slat chord ratio is in Family with slat sizing on current fleet commercial transport aircraft.

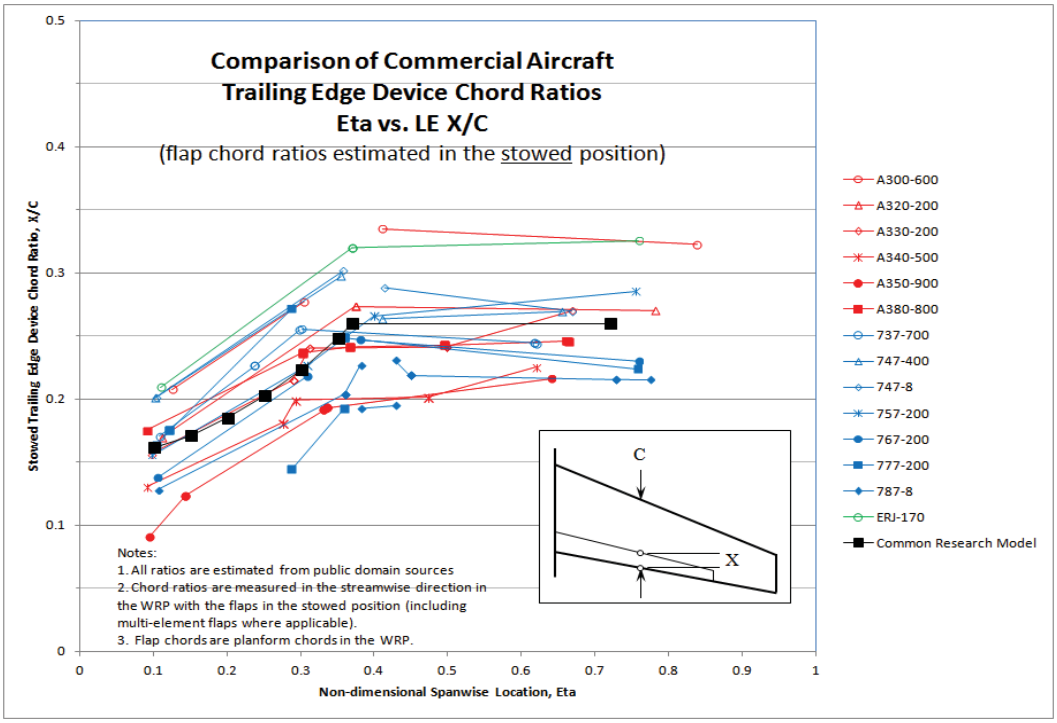

Figure 6 **CRM trailing-edge flap chord ratio is in family with sizing of similar trailing-edge devices on current fleet commercial transports.**

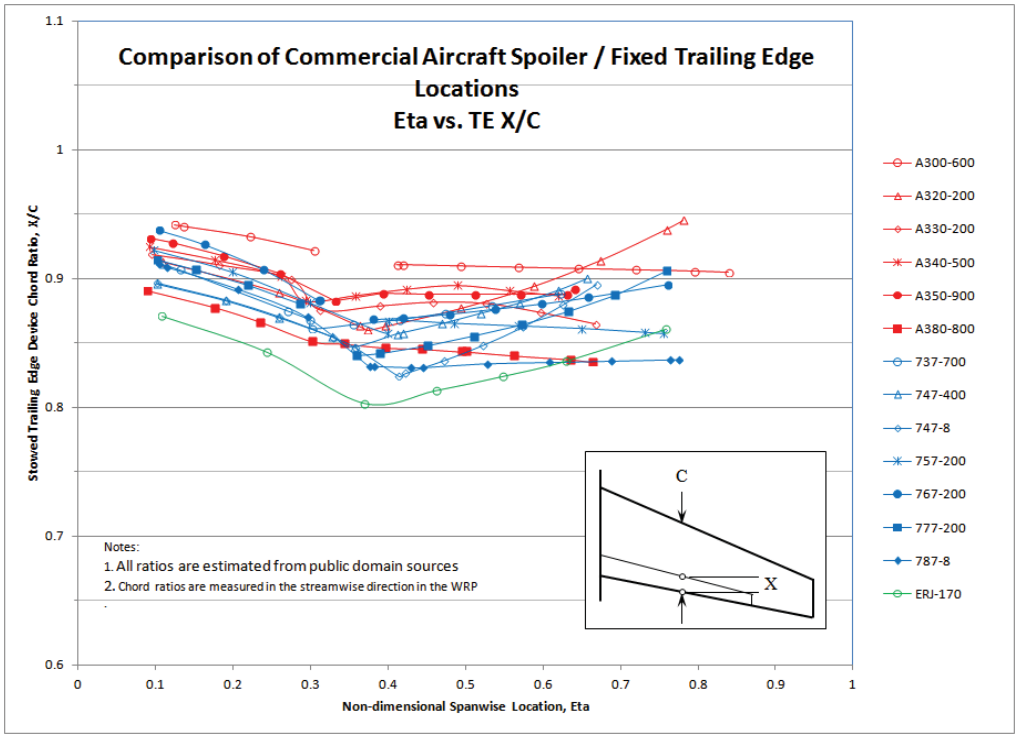

Figure 7 CRM spoiler-to-wing trailing edge chord ratio is in Family with control surface layouts on current fleet commercial transport aircraft.

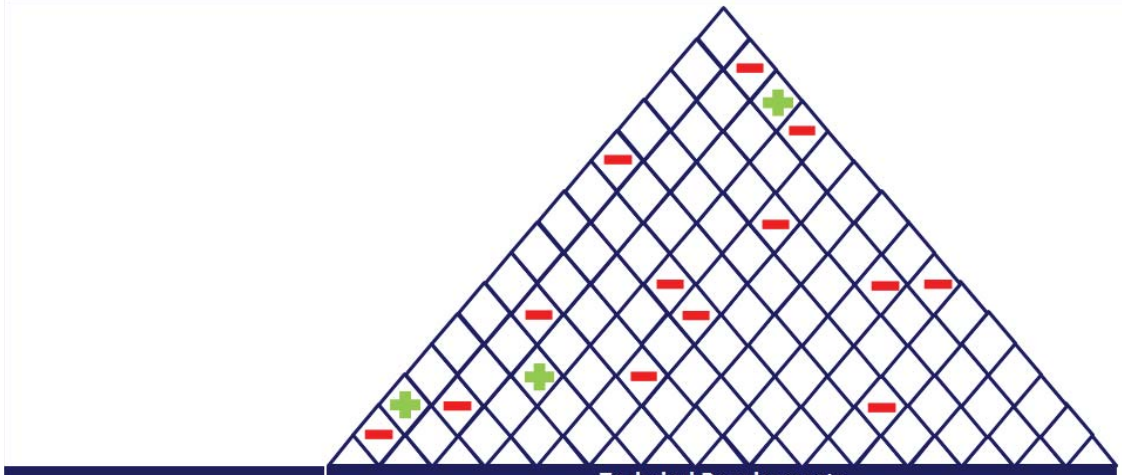

NASA Requirements	Weight (Scoring)	Technical Requirements: Producibility: Maintainability	Producibility: Mech. Systems Complexity	Producibility: Modularity	Producibility: Part Count	Design: Actuator Loads	Design: Derivative Potential	Design: Flight Controls	Design: Handling Characteristics	Design: Kinematicsa	Design: Power Requitrements	Design: Technical Risk (e.g., TRL level)	Regulations: Noise	Regulations: Handling Qualities	Regulations: Icing	Regulations: Redundancy	
Aerodynamic Performance																	
L/D for takeoff	24%	0	0	0	0	3	9	3	3	3	9	9	3	3	9	3	
Cl_{max} for landing	24%	0	0	0	0	3	9	3	3	3	3	9	9	3	9	3	
Environmental Impact													9				
High-Lift system acoustics	8%	0	1	0	0	3	3	3	1	3	3	9	9	0	3	0	
Engine emissions	3%	0	0	0	0	3	3	1	1	1	3	3	3	0	1	1	
Airplane Structures																	
Part count	24%	3	9	9	9	1	3	0	1	3	1	9	0	0	3	3	
Structural Weight	8%	1	3	1	3	3	3	1	3	3	3	9	3	3	1	3	
Mechanical complexity	8%	9	9	3	3	1	3	1	3	3	1	9	1	1	1	3	
Maintenance requirements	3%	9	9	1	3	1	1	1	0	3	1	3	0	0	3	3	
Technical Priorities		**1.7**	**3.4**	**2.5**	**2.7**	**2.3**	**5.8**	**1.9**	**2.2**	**2.9**	**3.7**	**8.7**	**3.9**	**1.7**	**5.5**	**2.7**	**TOTAL SCORE**
Conventional High-Lift Baseline	**Concept Scores**	2.0	2.0	2.0	2.0	2.0	4.0	4.0	4.0	2.0	2.0	5.0	1.0	4.0	4.0	4.0	72.9
Krueger + Simply-Hinged TE Flap		4.0	4.0	2.0	4.0	3.0	3.0	2.0	2.0	3.0	3.0	3.0	3.0	2.0	3.0	3.0	76.4
Morphing LE + Simply-Hinged TE Flap		4.0	5.0	2.0	5.0	4.0	3.0	2.0	2.0	4.0	3.0	1.0	4.0	2.0	2.0	2.0	81.6
Drooped LE + Simply-Hinged TE Flap		4.0	5.0	2.0	5.0	4.0	3.0	2.0	2.0	4.0	3.0	2.0	4.0	2.0	2.0	2.0	83.4
Krueger + Slotted TE Flap		3.0	3.0	2.0	3.0	3.0	3.0	2.0	2.0	3.0	3.0	3.0	2.0	2.0	3.0	3.0	69.5
Morphing LE + Slotted TE Flap		3.0	4.0	2.0	4.0	4.0	3.0	2.0	2.0	4.0	3.0	1.0	3.0	2.0	2.0	2.0	74.7
Drooped LE + Slotted TE Flap		3.0	4.0	2.0	4.0	4.0	3.0	2.0	2.0	4.0	3.0	2.0	3.0	2.0	2.0	2.0	76.4

Figure 8 QFD assessment of simplified high-lift systems is illustrated by a house-of-quality.

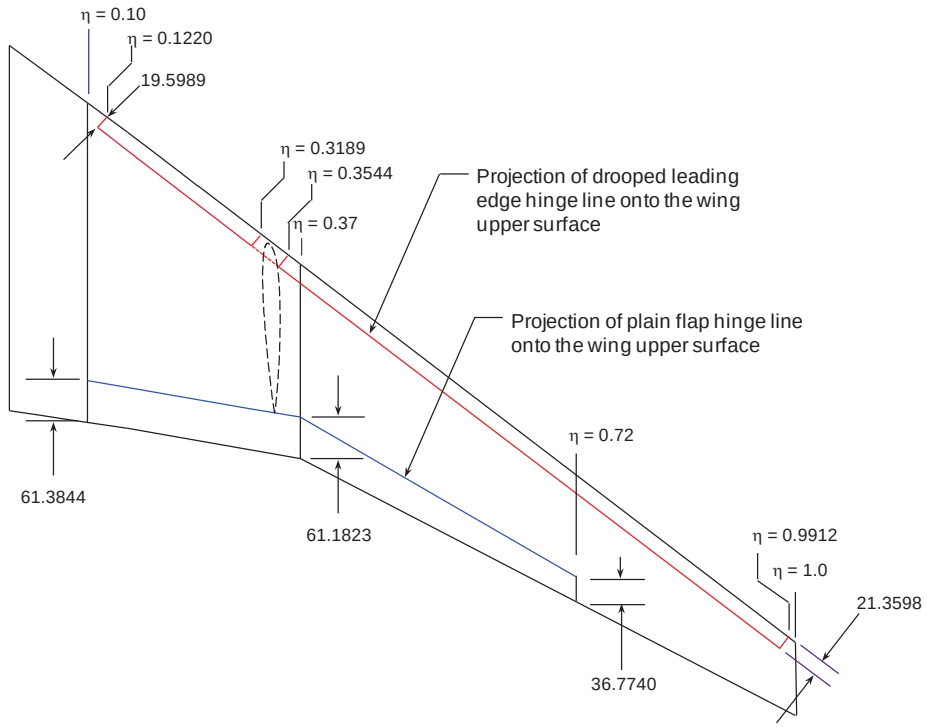

Figure 9 Conventional and simplified high lift system planform definitions are matched to promote meaning high-lift aerodynamics comparisons.

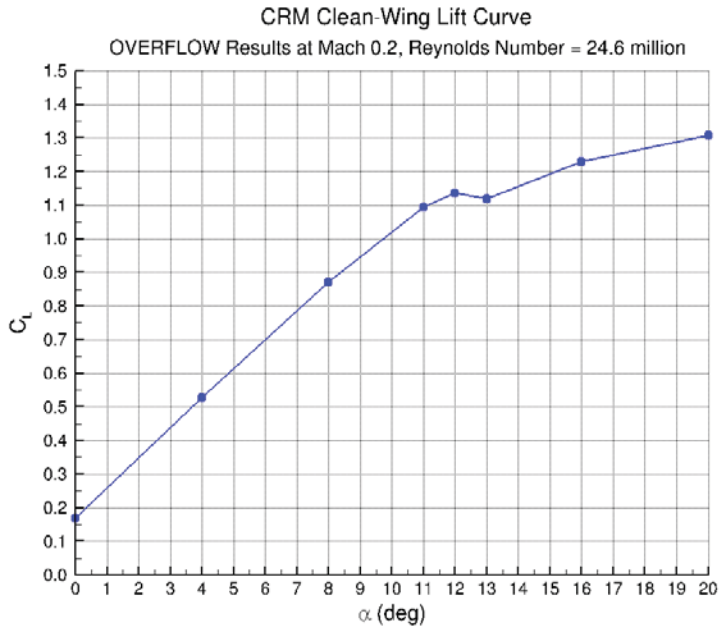

Figure 10 Variation of lift with angle of attack for a clean (i.e., all high-lift devices retracted) high-lift CRM wing/body/nacelle/pylon configuration..

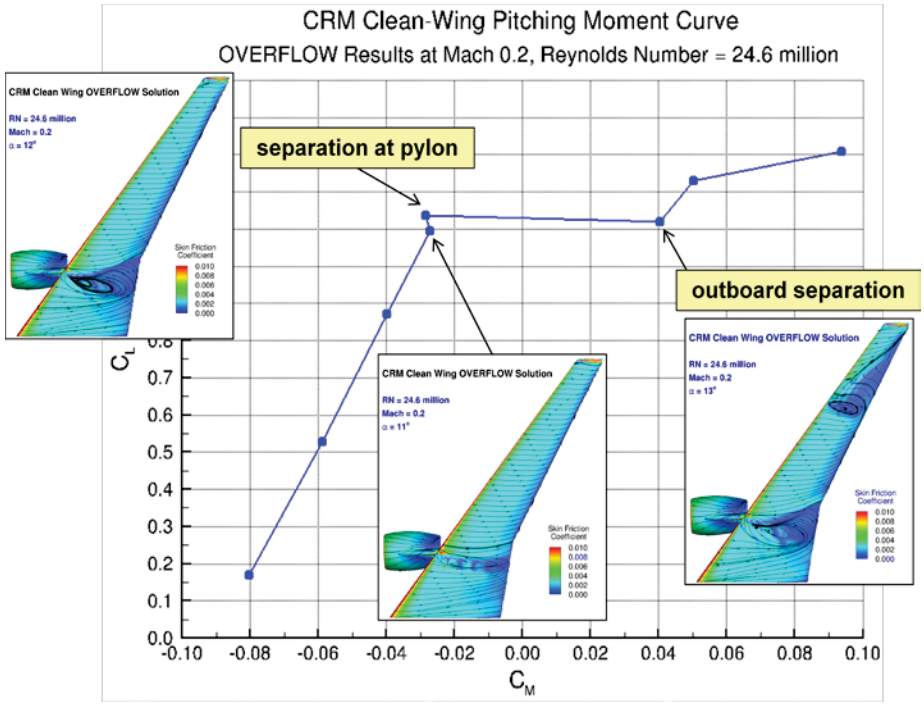

Figure 11 Lift-vs-pitching moment trace indicates progression in massive flow separation with increasing angle of attack.

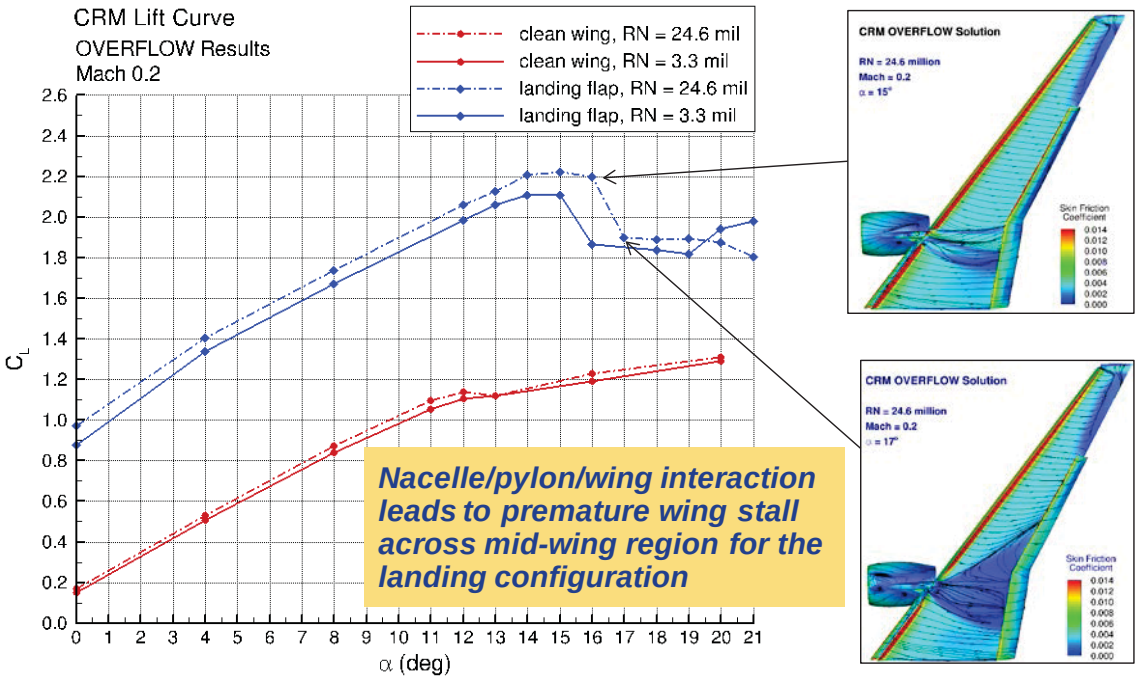

Figure 12 Surface flow visualizations aid in the explanation of stall characteristics of conventional high-lift CRM.

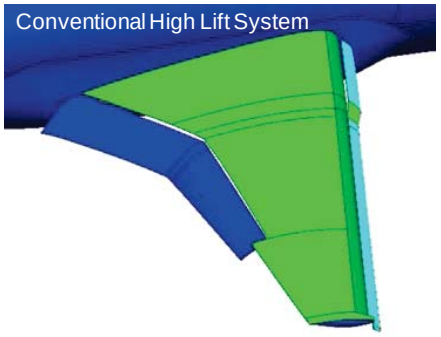

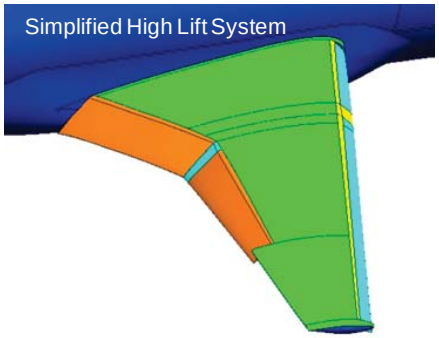

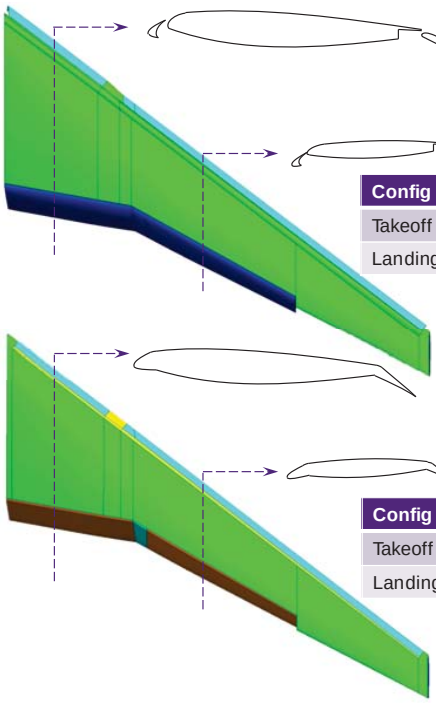

Config	δ_{SLAT}	δ_{FLAP}
Takeoff	18° / 25°	15°
Landing	18° / 25°	30°

Config	δ_{LE}	δ_{FLAP}
Takeoff	20° / 25°	15°
Landing	20° / 25°	30°

Figure 13 Wing/body definitions of conventional and simplified high-lift CRM variants.

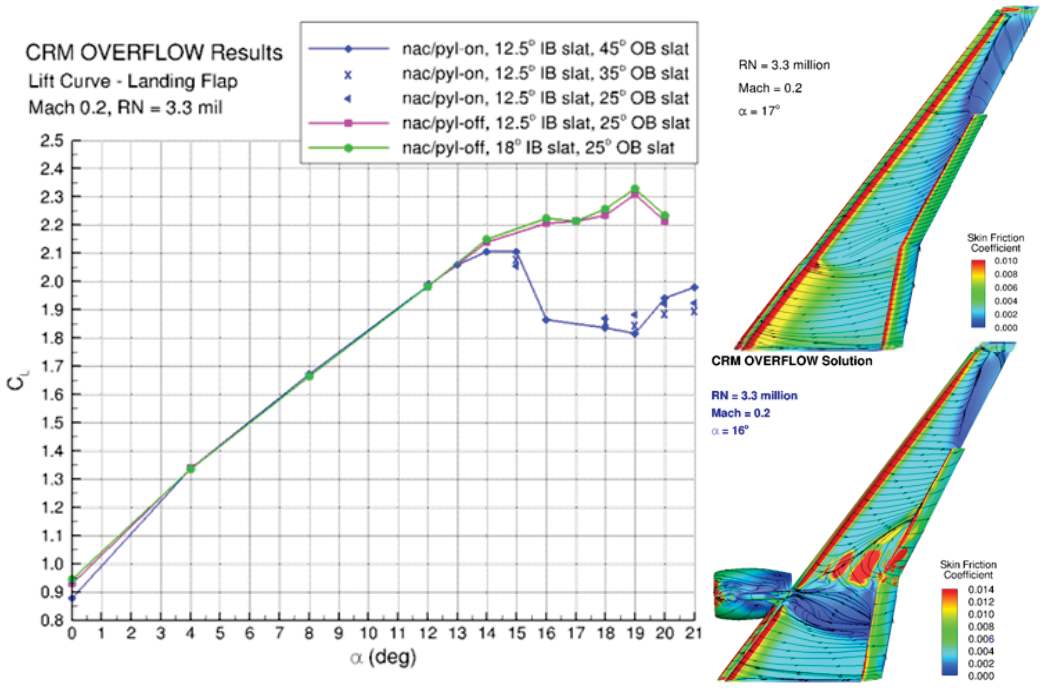

Figure 14 Wing/body high-lift CRM configuration eliminates massive nacelle-induced midspan flow separation and improves stall characteristics.

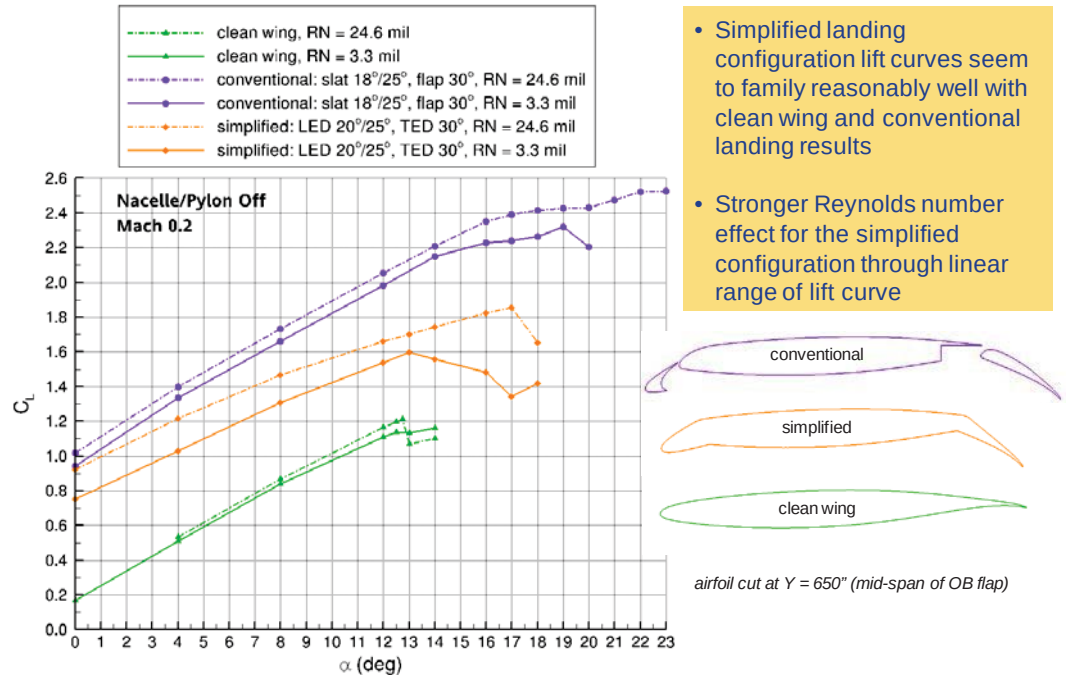

Figure 15 Lift curve comparisons – clean vs. landing-approach high-lift CRM configurations (conventional & simplified).

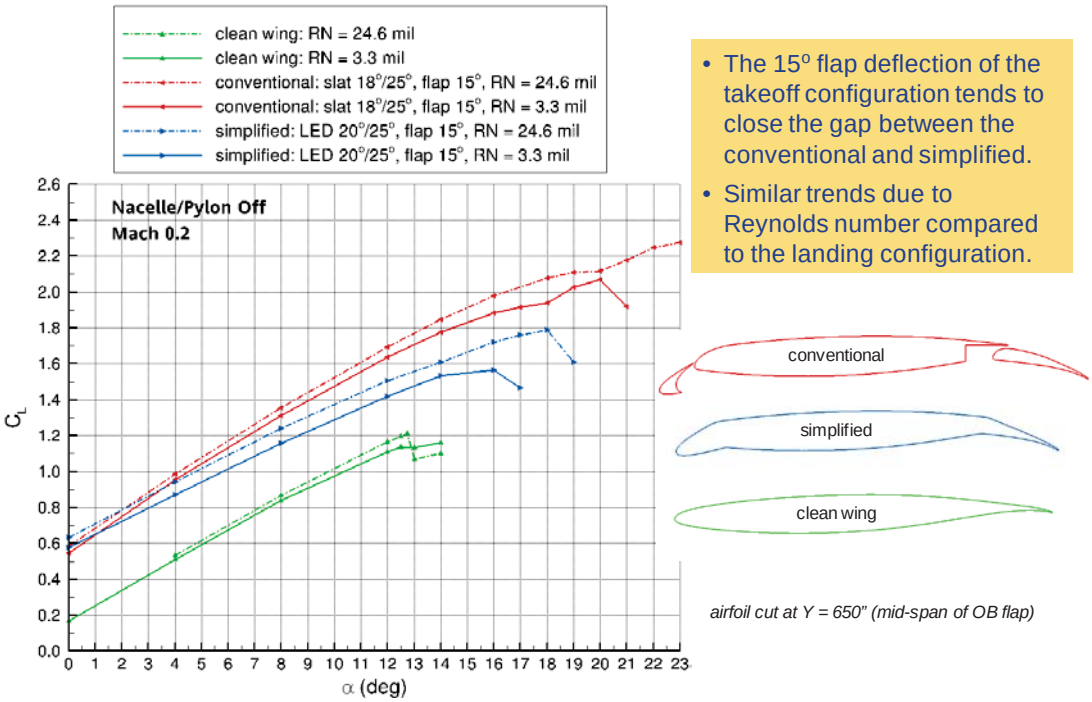

Figure 16 Lift curve comparisons – clean vs. takeoff high-lift CRM configurations (conventional & simplified).

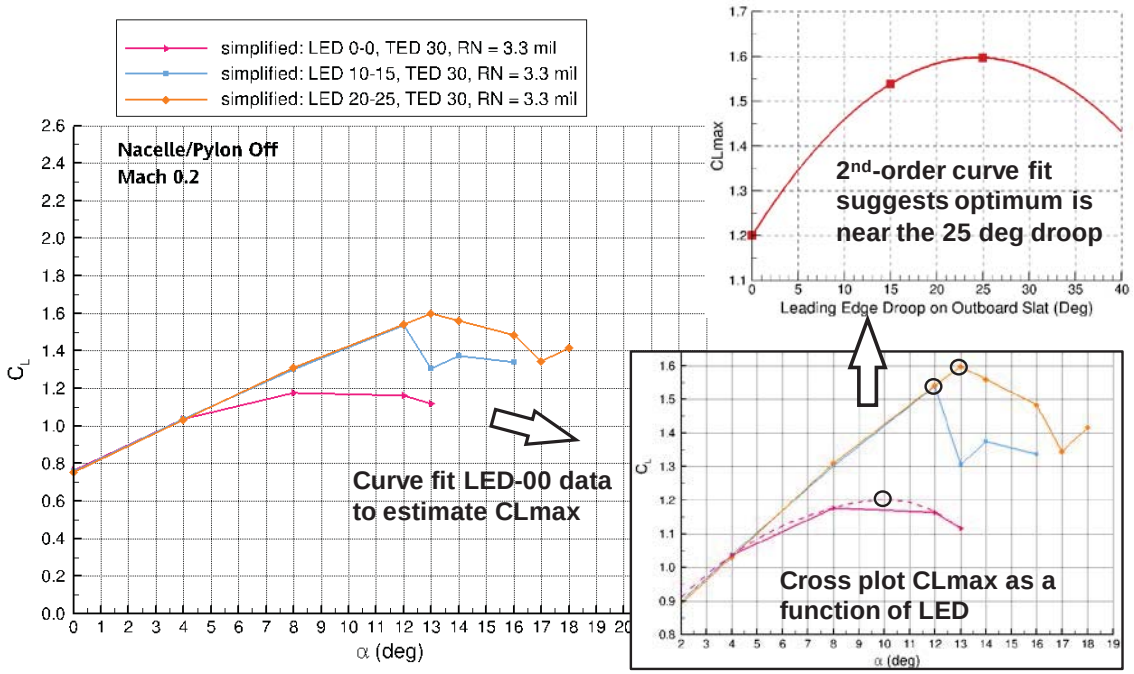

Figure 17 Lift curve comparisons for simplified high-lift CRM wing/body configuration indicate 25-degree leading-edge droop to be near optimum setting.

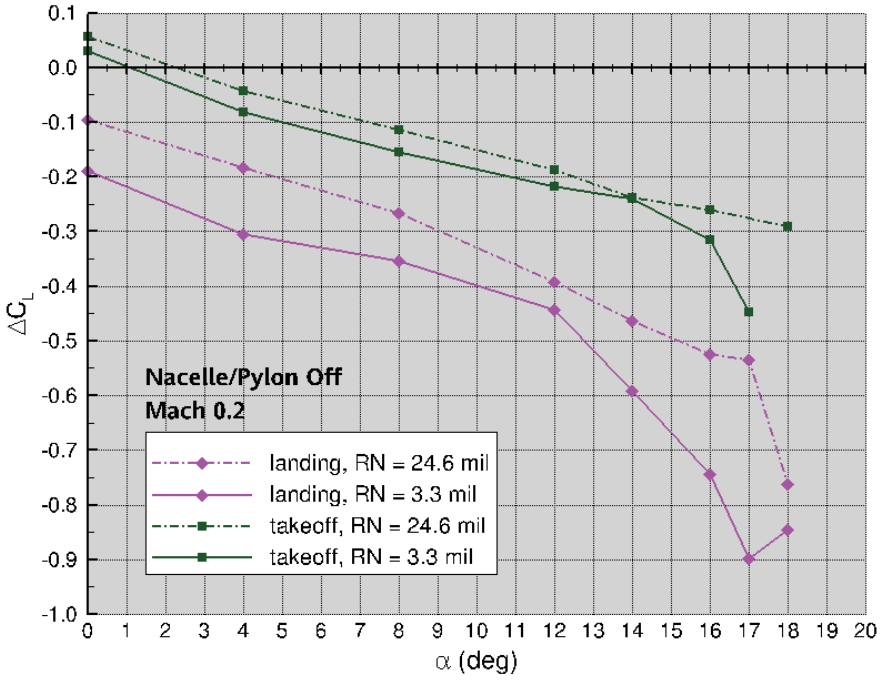

Figure 18 Incremental-lift comparisons between conventional and simplified high-lift CRM configurations.

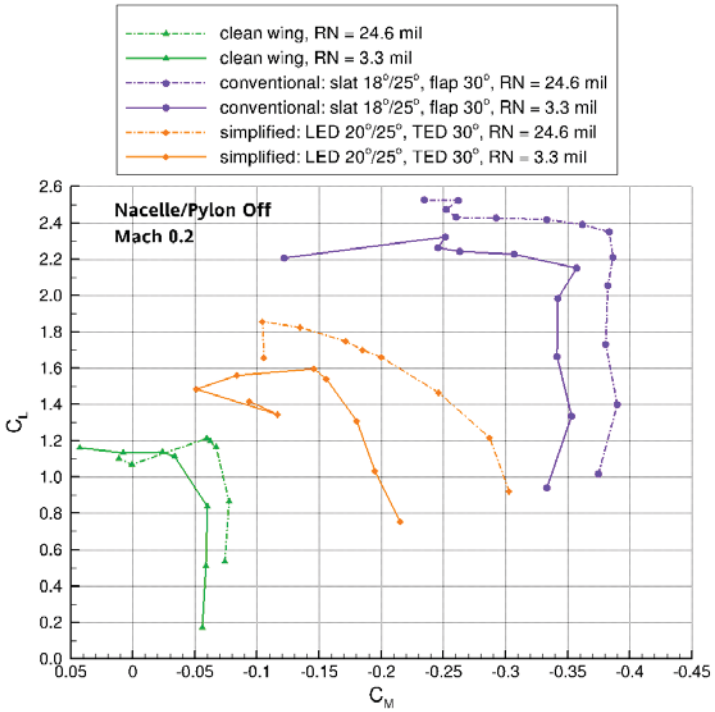

Figure 19 Pitching-moment comparisons – clean vs. landing-approach high-lift CRM configurations (conventional & simplified).

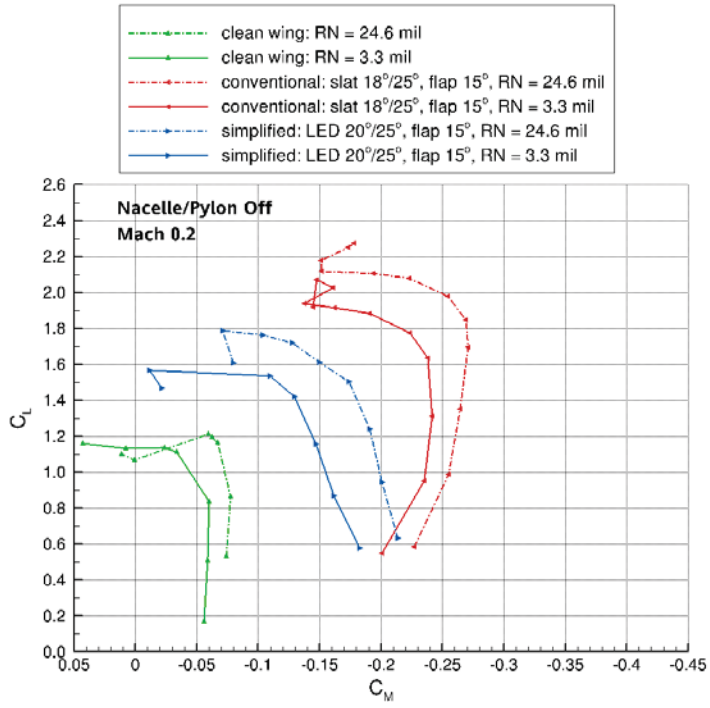

Figure 20 Pitching-moment comparisons – clean vs. takeoff high-lift CRM configurations (conventional & simplified).

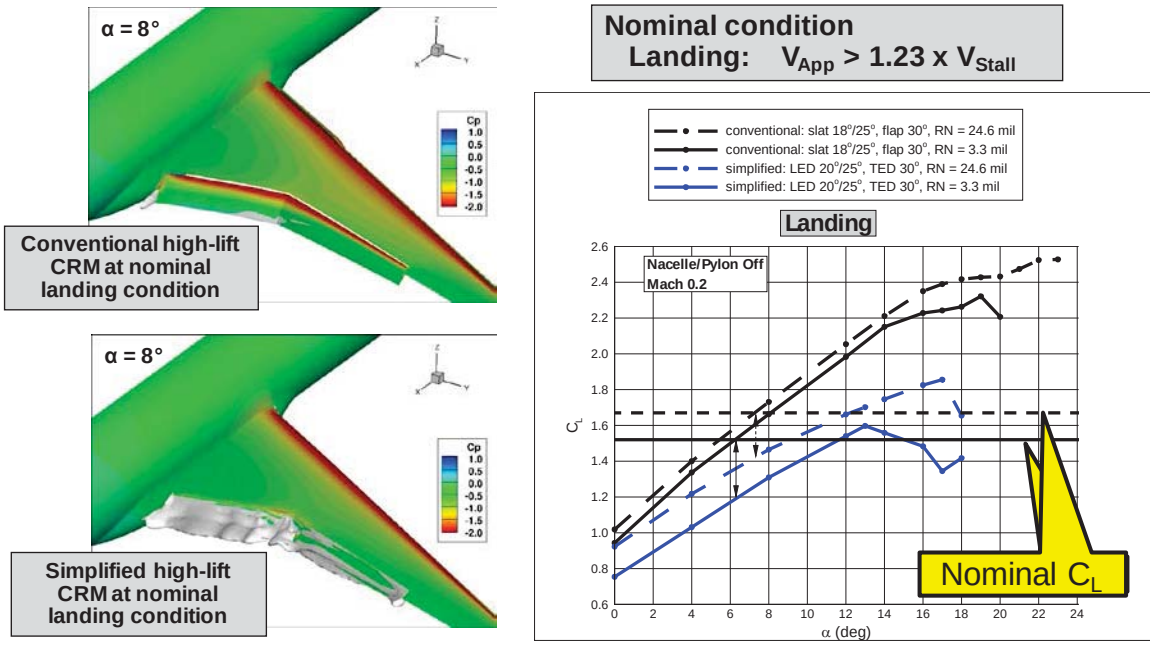

Figure 21 Nominal lift condition for landing-approach configuration is selected as reference condition for AFC integration trade studies.

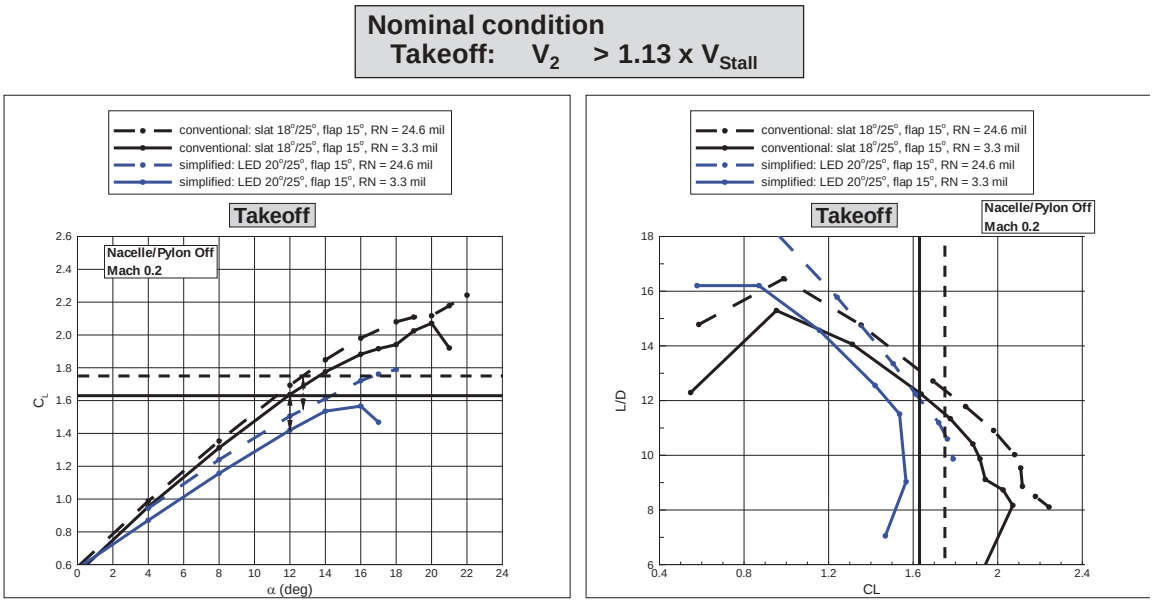

Figure 22 Nominal lift condition for takeoff configuration is selected as reference condition for AFC integration trade studies

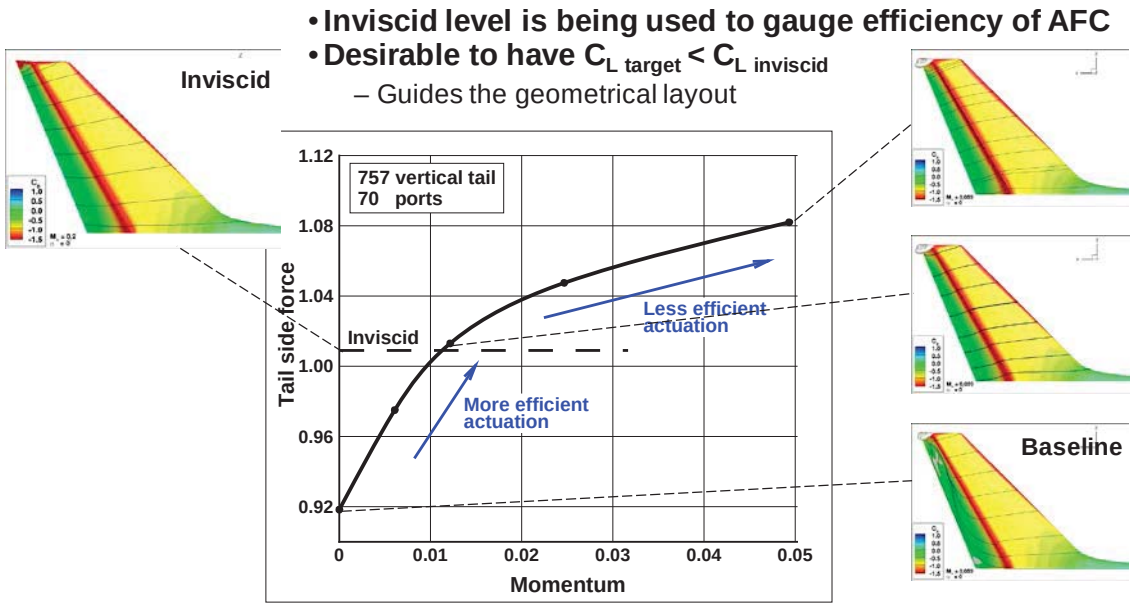

Figure 23 AFC is sized with inviscid limit solution

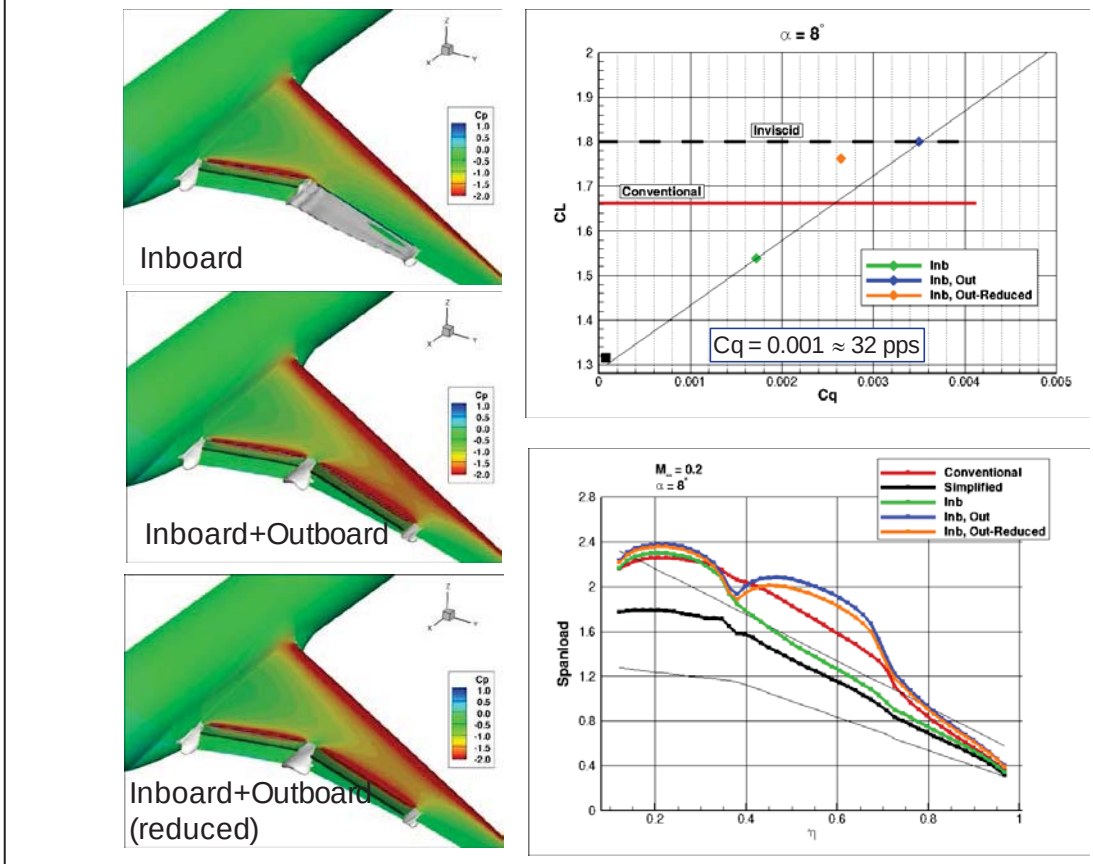

Figure 24 CFD solutions with constant-blowing boundary conditions identify approximate extent and mass flow rate for AFC high-lift application

- **AFC is placed on a backward facing step carved into the flap**
  - Vertical cut through the surface at jet location
  - Step height is scaled from AFC integration validated in recent NFAC wind-tunnel test of NASA B-757 vertical tail with AFC
- **AFC is applied at sections of the step**
  - Optional spanwise continuous jet or discretized jets

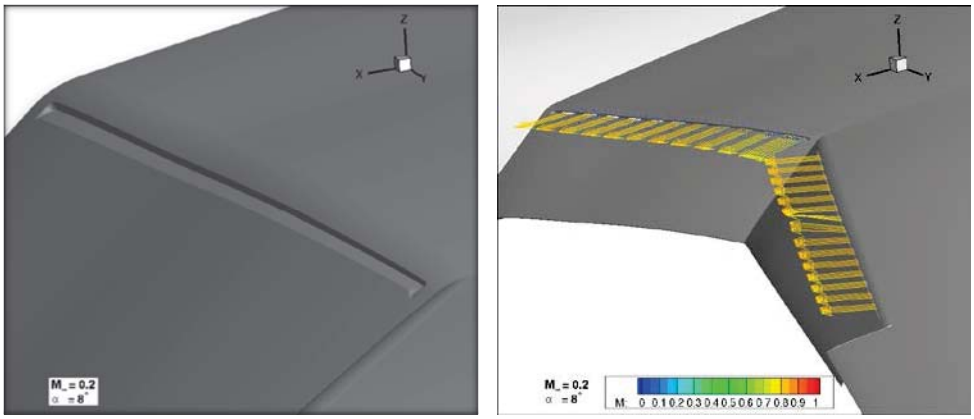

Figure 25 CFD study of AFC integration with NASA B-757 vertical tail guides present AFC application study.

- **37 ports in total**
  - 19 ports along inboard flap
  - 18 ports along outboard flap
- **Each port consists of a set of grids**
- **Trial-&-error used to guide orientation of discrete ducts to achieve desired Coanda effect for energizing the boundary-layer flow**

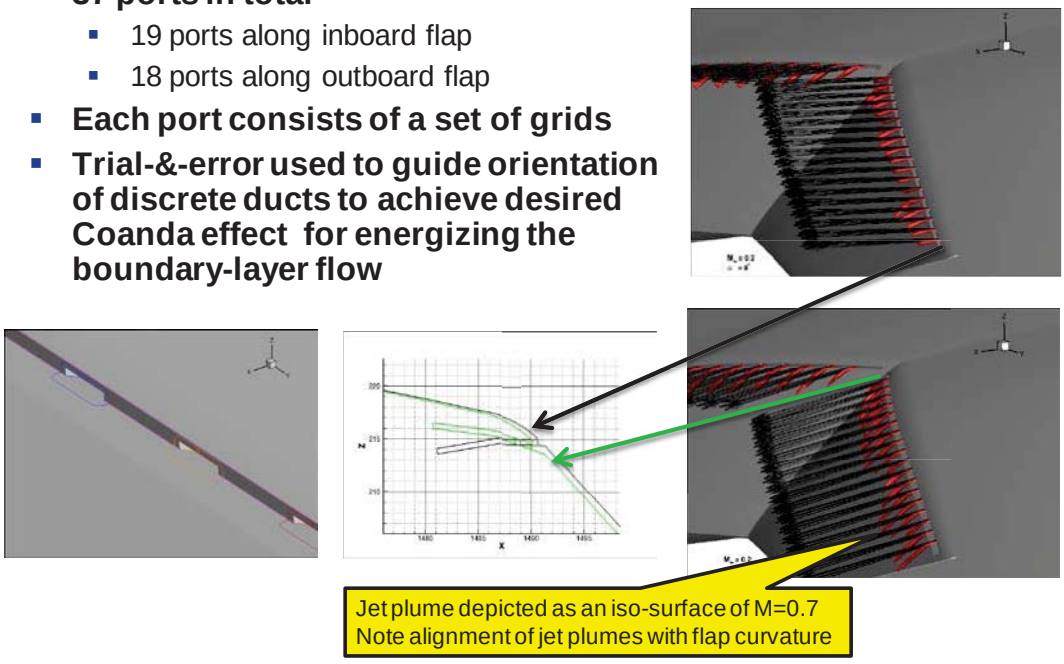

Figure 26 Convergent-divergent ducts are used to model fluidic oscillators for discrete-blowing AFC simulation.

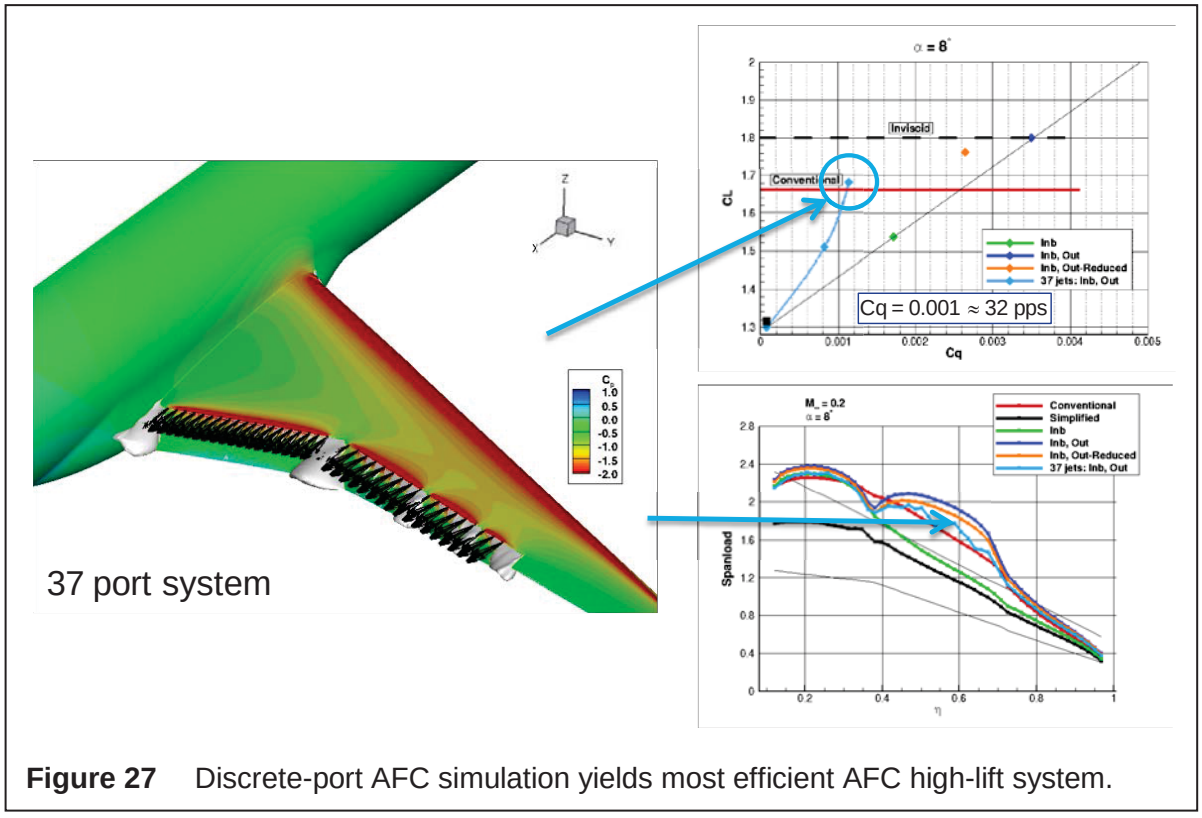

Figure 27 Discrete-port AFC simulation yields most efficient AFC high-lift system.

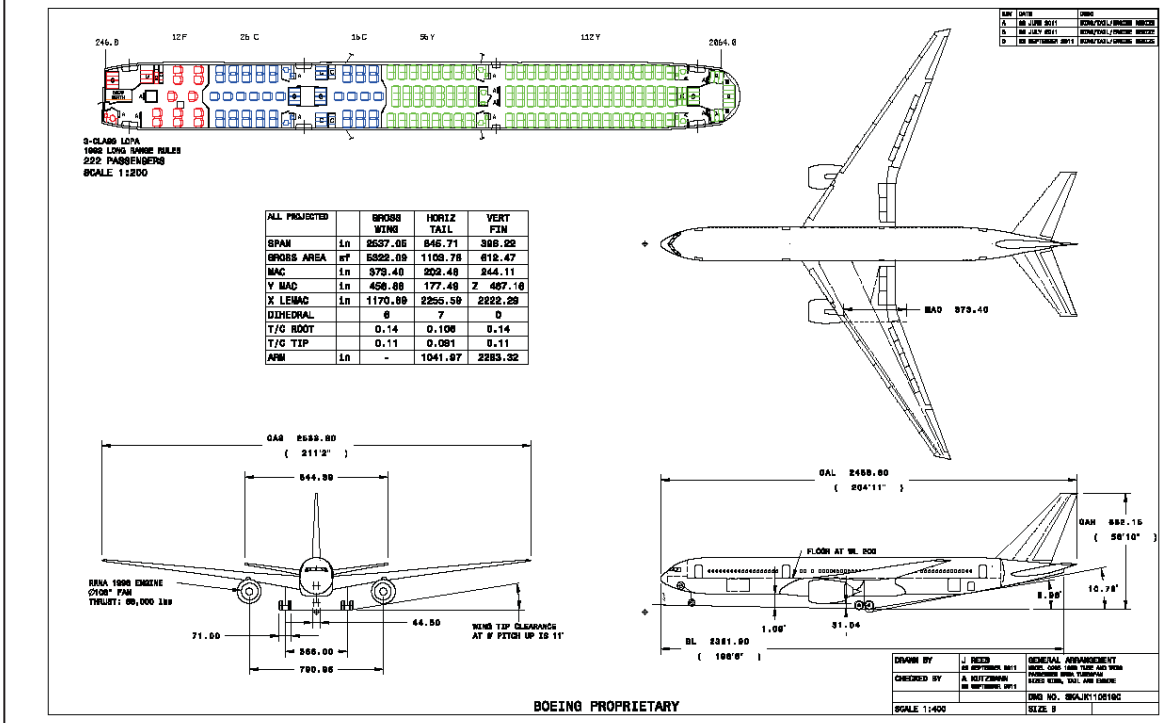

Figure 28 Trade studies are based on ERA-0003 concept since its mass properties are representative of CRM design.

			Baseline	AFC Enabled	AFC Enabled
			ERA-003-PAX	ΔFNto=-6952 lb	ΔFNto=-7254 lb
Reference	Required		1998 T&W	Unscaled	Sized FN & S
	Perf.		Mcr=0.85	Mcr=0.85	Mcr=0.85
			RR TF	RR TF	RR TF
MTOGW			581820	581820	587066
OEW			268686	268084	275240
Payload	50,000		50000	50000	50000
Fuel at Max PL			263134	263736	261826
Range (nm)	8000		8000	8143	8000
Block Fuel Burned			238569	239260	237149
Ton-nm/lbf			0.84	0.85	0.84
Wing Area, aero reference (sqft)			4960	4960	5350
Aspect Ratio, aero reference			8.7222	8.7222	8.7222
Span, aero reference (ft)			208.0	208.0	216.0
TO Ref FN @ SL, 0.0, +27F (lbf/eng)			88000	88000	90950
Number of Engines			2	2	2
T/W			0.30	0.30	0.31
W/S			117	117	110
Cruise type			Step-Cruise	Step-Cruise	Step-Cruise
Initial cruise altitude (ft)	35000		35000	35000	35000
Top of climb thrust (all engines, tau=1)			35122	35122	36299
Initial cruise Mach	0.85		0.85	0.85	0.85
Initial cruise L/D			19.372	19.650	19.66
Initial cruise SFC			0.5921	0.5921	0.5922
Initial cruise tau			0.833	0.821	0.802
Initial cruise CL			0.4536	0.4538	0.425
Distance to climb (nm)	200		199	193	179
Takeoff field length @ SL, 86F (ft)	10500		8657	9759	8656
2nd Segment Gradient (%)	2.4		2.527	2.444	2.452
Landing field length (ft)	5200		4168	4164	4049
Approach speed (ktas)	150		108	108	105

0.6% lower fuel burn

1.7% gain in range

1,110 ft TO field length penalty

Figure 29 Both sized and un-scaled AFC variants of ERA-0003 concept indicate potential for overall performance improvements.

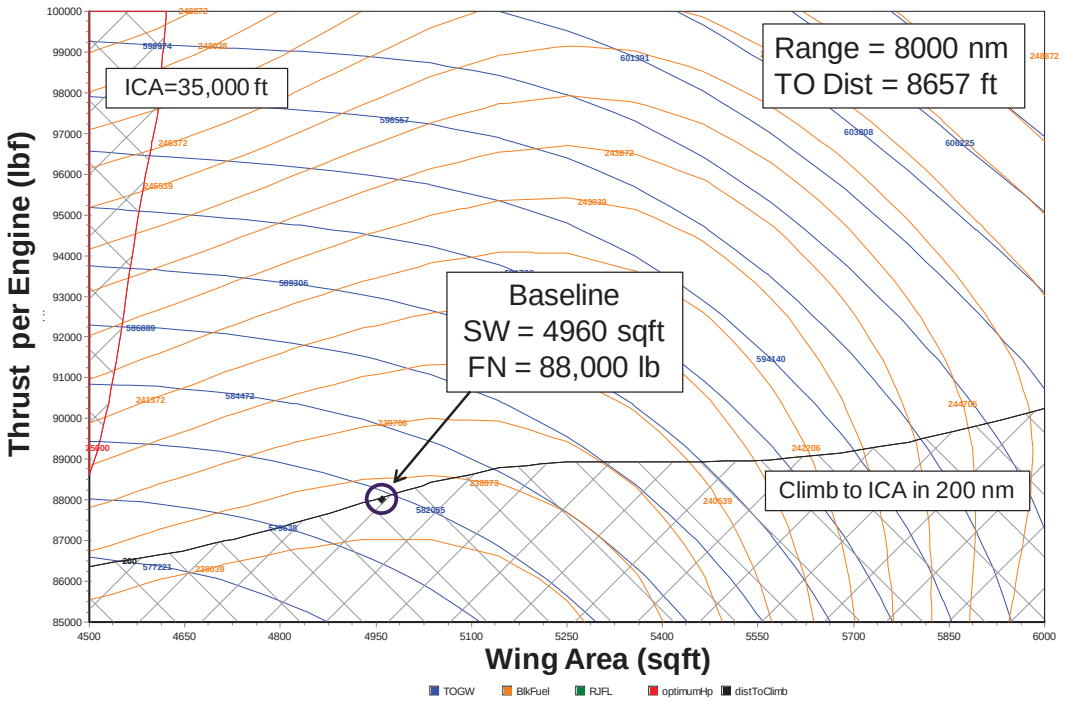

Figure 30 Climb-to-cruise requirement drives performance of baseline ERA-0003.

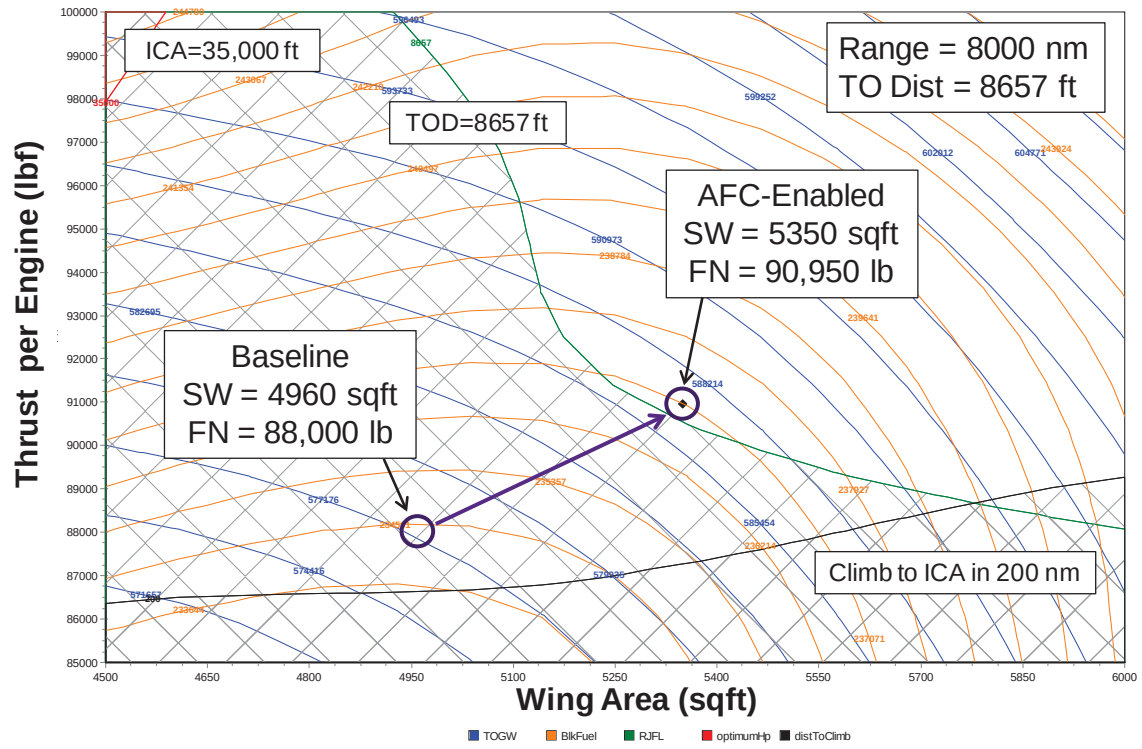

Figure 31 Takeoff field length requirement drives performance of AFC variant of ERA-0003.

REPORT DOCUMENTATION PAGE

Form Approved
OMB No. 0704-0188

1. REPORT DATE *(DD-MM-YYYY)*	2. REPORT TYPE	3. DATES COVERED *(From - To)*
01- 09 - 2014	Contractor Report	

4. TITLE AND SUBTITLE

AFC-Enabled Simplified High-Lift System Integration Study

5a. CONTRACT NUMBER

NNL10AA05B

5b. GRANT NUMBER

5c. PROGRAM ELEMENT NUMBER

6. AUTHOR(S)

Hartwich, Peter M.; Dickey, Eric D.; Sclafani, Anthony J.; Camacho, Peter; Gonzales, Antonio B.; Lawson, Edward L.; Mairs, Ron Y.; Shmilovich, Arvin

5d. PROJECT NUMBER

5e. TASK NUMBER

NNL13AB65T

5f. WORK UNIT NUMBER

473452.02.07.03.02.01

7. PERFORMING ORGANIZATION NAME(S) AND ADDRESS(ES)

NASA Langley Research Center
Hampton, Virginia 23681

8. PERFORMING ORGANIZATION REPORT NUMBER

9. SPONSORING/MONITORING AGENCY NAME(S) AND ADDRESS(ES)

National Aeronautics and Space Administration
Washington, DC 20546-0001

10. SPONSOR/MONITOR'S ACRONYM(S)

NASA

11. SPONSOR/MONITOR'S REPORT NUMBER(S)

NASA/CR-2014-218521

12. DISTRIBUTION/AVAILABILITY STATEMENT

Unclassified - Unlimited
Subject Category 34
Availability: NASA CASI (443) 757-5802

13. SUPPLEMENTARY NOTES

Langley Technical Monitor: John C. Lin

14. ABSTRACT

The primary objective of this trade study report is to explore the potential of using Active Flow Control (AFC) for achieving lighter and mechanically simpler high-lift systems for transonic commercial transport aircraft. This assessment was conducted in four steps. First, based on the Common Research Model (CRM) outer mold line (OML) definition, two high-lift concepts were developed. One concept, representative of current production-type commercial transonic trans-ports, features leading edge slats and slotted trailing edge flaps with Fowler motion. The other CRM-based design relies on drooped leading edges and simply hinged trailing edge flaps for high-lift generation. The relative high-lift performance of these two high-lift CRM variants is established using Computational Fluid Dynamics (CFD) solutions to the Reynolds-Averaged Navier-Stokes (RANS) equations for steady flow. These CFD assessments identify the high-lift performance that needs to be recovered through AFC to have the CRM variant with the lighter and mechanically simpler high-lift system match the performance of the conventional high-lift system. Conceptual design integration studies for the AFC-enhanced high-lift systems were conducted with a NASA Environmentally Responsible Aircraft (ERA) reference configuration, the so-called ERA-0003 concept. These design trades identify AFC performance targets that need to be met to produce economically feasible ERA-0003-like concepts with lighter and mechanically simpler high-lift designs that match the performance of conventional high-lift systems.

15. SUBJECT TERMS

Active flow control; Commercial transport; Common research model; High lift system; High lift integration; System integration

16. SECURITY CLASSIFICATION OF:			17. LIMITATION OF ABSTRACT	18. NUMBER OF PAGES	19a. NAME OF RESPONSIBLE PERSON
a. REPORT	b. ABSTRACT	c. THIS PAGE			STI Help Desk (email: help@sti.nasa.gov)
					19b. TELEPHONE NUMBER *(Include area code)*
U	U	U	UU	39	(443) 757-5802